ISSN 0736-5306

SCIENCE OF TSUNAMI HAZARDS

The International Journal of The Tsunami Society

Volume 4 Number 1 1986

copyright © 1986
THE TSUNAMI SOCIETY

OBJECTIVE: The Tsunami Society publishes this journal to increase and disseminate knowledge about tsunamis and their hazards.

DISCLAIMER: The Tsunami Society publishes this journal to disseminate information relating to tsunamis. Although these articles have been technically reviewed by peers, The Tsunami Society is not responsible for the veracity of any statement, opinion, or consequences.

EDITORIAL STAFF

T. S. Murty Technical Editor
Institute of Ocean Sciences
Department of Fisheries and Oceans
Sidney, B.C., Canada

Charles L. Mader - Production Editor
Los Alamos National Laboratory
Los Alamos, N.M., U.S.A.

George Pararas-Carayannis - Circulation
International Tsunami Information Center
Honolulu, HI, U.S.A.

George D. Curtis - President/Publisher
Joint Institute for Marine and Atmospheric Research
University of Hawaii
Honolulu, HI, U.S.A.

Submit manuscripts of articles, notes, or letters to:

T. S. Murty Technical Editor
Institute of Ocean Sciences
Department of Fisheries and Oceans
Sidney, B.C., Canada

If article is accepted for publication the author(s) must submit a camera ready manuscript. A voluntary $50.00 page charge will include 50 reprints.

SUBSCRIPTION INFORMATION: Price per copy: $20.00 USA Hardcopy

ISSN 0736-5306

Published by The Tsunami Society in Honolulu, Hawaii, U.S.A.

HEIGHT DISTRIBUTION OF THE TSUNAMI GENERATED BY THE NIHONKAI-CHUBU (JAPAN SEA CENTRAL REGION) EARTHQUAKE

Kinjiro Kajiura

Earthquake Research Institute
University of Tokyo
Yayoi, Bunkyo-ku
Tokyo, Japan

ABSTRACT

Inundation heights of this tsunami along the Japan Sea coast surveyed by many agencies in Japan are synthesized to give a general picture of height distribution and some characteristics of the distribution are discussed. First, the average height decays inversely proportional to the distance up to about 500Km from the source. However, in the far field in the western part of the Japan Sea, the decay of wave height do not follow a simple rule. Second, the local height statistics in the interval of about 40Km indicates that the height ratio of the maximum to the mean is about 2, and the ratio of the maximum double amplitude recorded on a tide gauge to the local mean height is between 0.5 to 2.0, confirming the statistics given by Kajiura(1983). Reflecting the smallness of the predominant period (less than 10 minutes) of this tsunami, the variability of height is significantly affected by small scale topography such as sand dunes and small harbours.

Introduction

As is already emphasized by Kajiura(1983), the observed values of tsunami run-up or inundation heights along the coast for a single event vary significantly not only regionally but also locally within a short distance and the maximum run-up height Hmax is about 2 times the average value for a coastal stretch of 20 Km along the Sanriku coast of northern Honshu. Therefore, we should be careful to interpret and utilize observed height values when the "representative" height value is required in practice. Because of the advance of technique to simulate a real tsunami by numerical means, it is increasingly important to understand the statistical characteristics of local variability of wave height along the coastal area which is not well resolved in the framework of an assumed numerical model. Furthermore, the local risk analysis of tsunami to be used with advantage, it is also necessary to take these spacial variabilities into account. In the present paper, we analyzed data of tsunami run-up heights along the Japan Sea coast at the time of Nihonkai-Chubu Earthquake on May 26, 1983, to elaborate the discussion on spacial statistics already made for tsunami heights observed along the Pacific coasts of Japan (Kajiura,1983).

Outline of the Tsunami Accompanying the 1983 Japan Sea (Nihonkai-Chubu) Earthquake

The Japan Sea Earthquake (M7.7, JMA) occurred on 26 May 1983 at 12:00 JST about 100Km off the coast of Akita Prefecture in northern Honshu. The tsunami source area was delineated by travel times of the tsunami front to several tide stations and estimated to lie offshore of the northern Honshu enclosing the epicenter of the earthquake with the N-S length of 140 Km and E-W width of 90 Km (Hatori,1983; PHTRI,1983; JMA,1984). The western half of the tsunami source is located in the deep sea 2000 m to 3000 m deep, and the eastern half lies on the continental slope area with the eastern margin reaching almost to the edge of the shelf at 200 m isobath. The predominant period of this tsunami was 8 to 10 minutes and very large run-up was observed in the northern Akita coast.

The aftershock area of this earthquake corresponds to the western half of the tsunami source area with the length 120 Km and the width 30$\sim$35 Km (Noritomi,1984). The total seismic moment Mo of this earthquake estimated from long-period seismic surface waves is about $7.5*10^{27}$ dyne·cm (Satake, 1985) in contrast to about $3.5\sim4.8*10^{27}$ dyne·cm estimated from body wave analysis (JMA,1984; Noritomi,1984) and two eastward dipping ($20^{\circ}\sim30^{\circ}$) shallow thrust faults (total dimension, $100\sim120*40$ Km^2) corresponding to the aftershock area are proposed (JMA,1984; Satake,1985). Based on a simulation model of the tsunami, Aida(1984) determined most likely parameters of the tsunami source compatible with both the earthquake and tsunami data. In his model, Mo is $5.8*10^{27}$ dyne · cm. The moment magnitude of this earthquake, Mw is about 7.8 to 7.9 and somewhat larger than the JMA magnitude. Amount of slip on the fault is about 5 to 7 m in the southern fault plane and about 4 to 5 m in the northern one. The total tsunami energy Et based on these fault models is about $4*10^{20}$ ergs (Aida,1984; Satake,1985).

A special feature of these fault models is that the rigidity μ is considered to be smaller ($3\sim4*10^{11}$ dyne·cm^{-2}) than that for the thrust type fault models for the Pacific earthquakes ($5\sim7*10^{11}$ dyne·cm^{-2}), so that the total tsunami energy Et is about twice as large as those of the Pacific tsunamis for the same earthquake moment Mo. This situation of the larger tsunami potential for the Japan Sea earthquakes was discussed by Abe(1985) in terms of the tsunami magnitude Mt defined by him. For the Japan Sea tsunamis, Mt determined from tsunami data alone is about 0.2 larger than the moment-magnitude Mw of earthquakes, which is equivalent to about 2.5 times larger tsunami energy according to the formula given by Kajiura(1981).

Data

The results of field survey of tsunami run-up height were reported by many research groups, such as the Japan Meteorological Agency (JMA,1984), the Port and Harbour Technical

Research Institute (PHTRI,1983), the Public Works Research Institute (PWRI,1985), National Research Center for Disaster Prevention (NRCDP,1984) and University Research Group (ESTE: Experimental Station for Tsunami Engineering,1984). The weight of survey was placed differently depending on their specialized field of research and the data are more or less complementary. For example, the Port and Harbour Technical Research Institute (PHTRI) made a detailed survey of tsunami height distribution mainly in the vicinity of port and harbour areas, in contrast to the Public Works Research Institute (PWRI) which concentrated its effort in clarification of tsunami behaviours along the extended coastal area in northern Akita Prefecture, where the run-up was the highest and damages to shore protection works were severe. Groups of Japan Meteorological Agency (JMA), National Research Center for Disaster Prevention (NRCDP), and Universities (ESTE) covered a wide area of the Japan Sea coast to see the gross distribution of tsunami height. In particular, Tsuji of NRCDP (Tsuji et al.,1985) collected information of tsunami inundation along the Japan Sea coast of southern Korea with the collaboration of Korean scientists.

Relevant tide gauge records were collected and disseminated by several groups (JMA,1984; PHTRI,1983; PWRI,1985; Hatori,1983; etc). In these reports, the arrival time of wave front, initial wave amplitude, maximum double amplitude (trough to crest height) with its time of appearance were tabulated for each tide station. More than 60 tide stations are listed but near the tsunami source, no reliable tsunami records was obtained.

In the present paper, the observed tsunami heights reported by the University Research Group (ESTE,1984), JMA(1984), NRCDP(1984) and PHTRI(1983) are mainly used to discuss statistical behaviours of overall tsunami height distribution along the coast of Japan. And for the discussion of the local run-up height distribution at the Minehama coast, PWRI(1985) data are used.

Method

The Japan Sea coasts from Wakkanai in the northern most location in Hokkaido to Yamaguchi Prefecture in the western end of Honshu are divided into segments about 40 Km long as shown in Fig.1. The numbering of each segment follows the identification number of maps showing tsunami heights in the report by the University Research Group (ESTE,1984) except for No.76 to No.82. In Fig.1, the location of the earthquake epicenter (40.4° N, 139.1°E) is also shown.

In each segment n, all the observed inundation height values are averaged logarithmically in principle to give a single value $\tilde{H}n$ and the standard deviation SDn (logarithmic). However, when the sampling density of data are inhomogeneous and several data are reported from a limited small area, those data are lumped together to avoid bias in the averaging in the segment as far as possible.

Here, it is mentioned that, along the Japan Sea coast, the datum level of land survey T.P., which is roughly the mean sea level in Tokyo Bay, is lower than the local mean sea level (M.S.L.). On the other hand, since the tidal range in the Japan Sea is small, the datum level for maritime construction works (C.D.L.) is only about 15 to 20 cm below M.S.L. in many places. The level of T.P. is 5 to 10 cm below M.S.L. in Hokkaido and about 17 cm below M.S.L. to the west of Toyama Prefecture, where the T.P. level is almost the same as C.D.L. However, on the coast in the northern Honshu from Niigata city up to Aomori Prefecture, T.P.levels are very often about 20 to 30 cm below M.S.L. and 10 to 15cm below C.D.L. so that the tsunami height values referred to T.P. in this area are correspondingly larger than the values referred to M.S.L. The monthly mean sea level in May coincides approximately with M.S.L. averaged over a year and the time of earthquake occurrence was about 2 hours before high tide in the northern Japan Sea. The final values reported by the University Research Group are based on T.P. and JMA reports very often the deviation of sea levels above the ordinary tide level (which is almost the same as M.S.L.), NRCDP used M.S.L. and PHTRI used C.D.L. However, in the following, we do not make any correction to given height values. It is conceivable that the difference of up to 30 cm may exist in the height values along the coast of northern Honshu, but in these

regions the tsunami height is relatively large so that the relative error due to the difference of the reference levels may be neglected.

Statistics

A summary of data for each segment is given in Table 1. In this table, the number of samples denoted by N* is that already processed beforehand, but the maximum and minimum heights are for the original total samples denoted by N, provided that the data obtain in the upstream of rivers are omitted from the beginning. Total number of data is 1396. Since all averaging was made logarithmically, the standard deviation SDn is that of log H in the nth local segment. Now, for the coast of the Japan Sea the overall distribution of average tsunami heights $\widetilde{Hn}$ together with the standard deviation is shown in Fig.2. In the figure, the data for islands and also for the Pacific Ocean side are omitted to see the distribution along the Japan Sea coasts more clearly. The segment numbers shown in the figure are in order from the north: 2-3, 5-15, 17, 33-39, 41-42, 47-56, 58-73, 76-80 and about 1500 Km in straight length. In this case, the number of processed data is 487.

It is interesting to notice that the mean value $\overline{SDn}$ of all SDn shown in Fig.2 comes out to be 0.161 which is almost the same as the average of $\overline{SDn}$ ($\langle SDn \rangle \sim 0.160$) given in the previous investigation; namely, the ratio H/Hn lies mostly between $0.5 < H/Hn < 2.0$ (less than $2\overline{SDn}$) in each segment. It is remarked here that the length of the segment is now 40 Km for the whole Japan Sea coast of about 1500 Km, in contrast to the previous investigation where the segment length was about 20 Km over the coastal area of length 300 Km.

The maximum value of $\widetilde{Hn}$ denoted by $\widetilde{Hn}max$ is 7.5 m found in the northern Akita coast (No.36). For a stretch of about 300 Km near the center of tsunami attack from a southern tip of Hokkaido to the southern border of Akita Prefecture (No.17 to No.39), the average height $\widetilde{H}$ is 2.81m with the mean standard deviation MSD=0.20 (logarithm) and $\overline{SDn}$=0.145. The combined total standard deviation SDT for the coast of 300 Km computed by $SDT^2=(MSD^2+\overline{SDn}^2)$ becomes 0.25, which is about the same as $\langle SDT \rangle = 0.24$ which is the average of SDT for 6 tsunamis in the Pacific. The ratio $\widetilde{Hn}\,max/\widetilde{H} = 2.67$. This height ratio indicates that the present tsunami showed somewhat higher run-up in the central segment (No.36) as compared with the case of average tsunamis for which $\widetilde{Hn}\,max/\widetilde{H}$ is around 2 (Kajiura,1983). This point will be discussed later. However, the scatter of data in each segment indicated by SDn is in the range expected from past experience.

It is seen in Fig.2 that the height distribution from south Akita to Toyama Prefecture is similar to the distribution in the northern Japan with height values of about 0.3 m at Toyama (No.53) and Wakkanai (No.2). In contrast, to the west of Noto Peninsula, the heights do not decay with distance so simply.

Decay of Wave Height With Distance

Decay of tsunami height $\widetilde{Hn}$ with distance is examined by plotting the average tsunami height $\widetilde{Hn}$ (in meter) in each segment as a function of distance, in which distance Δn is measured along the shortest oceanic path in Km from the earthquake epicenter to the center of each coastal segment. According to Fig.3, the inversely linear relationship between the average tsunami height $\widetilde{Hn}$ and distance Δn is evident in a range of about 500 Km: in the northern segments, almost up to Wakkanai (No.2), and in the south-western segments, up to Toyama (No.53). However, beyond Noto Peninsula, the scatter of data is very large. Recalling that, in tide gauge records, the maximum double amplitudes appear several hours later than the front arrival in many stations in the western Japan, it is probable that a single decay law does not apply to the maximum wave in these areas. The straight solid line and dashed lines in the figure are drawn by the formula

$$\log \widetilde{Hn} = -\log \Delta n + 2.50 \pm 0.2 \qquad (1)$$

Except for the highest value at the segment 36, most of data are within the range given by (1). However, in the northern branch, the negative deviation is relatively large in the segment group A surrounded by a dashed line in the figure. The location of this group A (segment number 2,3,8)is along the northern Hokkaido coast facing a wide continental shelf and is more or less in the shadow zone of Shakotan Peninsula. In the southern branch, the notable negative deviation is seen in the group B (segment number 53,54,55,61) and the positive deviation in the group C (segment number 66,68,72,73,76,79). The location of the group B is behind Sado Island with respect to the incoming tsunami, except for the segment 61 which is in the shadow of Noto Peninsula. On the other hand, the segments belonging to the group C are distributed along the coast of western Japan, indicating that the maximum wave heights were enhanced by some reasons in these areas. In particular, the tsunami height was large along the coast of Shimane Peninsula (segment number 72,73,76), which is in parallel to relatively large tsunami height in Oki Island (segment number 74). Here it is remarked that, along the Korean coast between 37°~38°N, the height of this tsunami was unusually large: the maximum height at Imwon was about 4m (Tsuji et al.,1984). Although not so distinct, the segments 38 to 42 to the south of Oga Peninsula show somewhat smaller run-up heights, possible because of the topographic effects. The wave heights on islands given in Table 1 show that the heights are above average in most of islands.

It is mentioned here that Abe(1985) analyzed the dependence of the maximum double amplitude H2 recorded on tide gauges to the distance Δ from the epicenter to the station and gave the average tsunami magnitude Mt for the Nihonkai-Chubu earthquake as Mt=8.1. Recalling that the relation between H2 and Mt is: $Mt = \log H2 + \log \Delta + 5.55$, the constant term becomes 2.55 (More accurately the average Mt computed from his Table III is Mt=8.07±0.2 so that the constant is 2.52). This constant term indicates that the ratio $H2/\widetilde{Hn} \sim 1.1$, which is consistent with the past experience (Kajiura,1983) that the ratio of the maximum double amplitude H2 observed by a tide gauge to the average run-up height $\widetilde{Hn}$ in the vicinity is scattered between 0.5 to 2.0 with the logarithmic mean value around 1.0. In Fig.4 the ratio $H2/\widetilde{Hn}$ for the present tsunami is plotted as a function of $\widetilde{Hn}$ and again it is confirmed that the mean value of this ratio is about 1.0. (In the figure, H2 values given by JMA(1964) are used so that the definition of H2 is slightly defferent from Abe's H2).

Run-up Height in Northern Akita Coast

The maximum run-up height for this tsunami was observed in Minehama district in the northern Akita coast. This sandy coast is facing a shallow sea with the bottom slope of only 1/200 or so up to about 30 Km offshore. On land, well developed sand dunes with the crest height more than 10 m line up about 100 to 200 m inside from the shore line and several small rivers cut the dune and forming relatively flat land. The waves invading on this coast were distinct in that the waves were disintegrated into short period waves during propagation and finally formed breakers. The situation is well investigated by Shuto (1984) and many photographic records are available. The traces of the wave run-up on sand dunes and flat lands were carefully followed and measured by means of skilled interpretation of areal photography and also on site levelling survey (Akita Prefecture,1984; PWRI,1985)

One representative area of Minehama in which the maximum run-up height of 14.93m was observed is shown in Fig.5 (This value is larger than that listed in Table 1). The line of inundation limit shown in the figure are determined by means of both on site inspection and areal photography. Including this area, a stretch of sandy coast of about 10 Km up to Agano River to the south was the place where most violent attack of tsunami occurred.

In Fig.6 the run-up or inundation heights actually measured (above T.P.) in this area (Fig.5) and also in the area of Tako River about 1 Km to the south of this area are shown as a function of location from the shore line. Because of the existence of relatively high sand dunes, high run-up values are found mainly in the distance 100 to 150 m from the

shore-line. The tsunami invades inland overflowing sand dunes when the dune height is less than about 10 m and also along river channels. In the areas of flat land along rivers, the water flows inland for a considerable horizontal distance, but the inundation height itself is not so large. Therefore, the final height of tsunami observed at the inundation limit is seen to diminish with distance. This shows that both the tsunami run-up height on land and the distance of horizontal inundation change drastically depending on the local topography on land, terrain slope and the degree of roughness. If there were no sand dunes and the terrain slope were small in this coastal area, the maximum run-up height would have been much lower than that actually observed.

Regarding the local variability of tsunami heights, it is also remarkable that the heights inside of small fishing harbours were reduced considerably in many places. Related to this reduction of heights, the effects of breakwater opening, crown height of breakwater, area and configuration of the harbour and the presence of sea walls were discussed (PHTRI,1983). Roughly speaking, the ratio of the heights inside and outside of the harbour is between 1.0 to 0.4 if the parameter $A/(T\sqrt{gh})$ is larger than, say, 10^{-3} where A is the harbour area, T is the tsunami period, and h is the mean depth of the harbour(PHTRI,1983,Fig.8・12). Also, within the relatively large port area of Noshiro (about 4Km long), the tsunami inundation heights were between 2 to 4.5 m in contrast to the estimated height of about 6m outside (PWRI,1985).

Concluding Remarks

From a deterministic point of view, the spacial distribution of tsunami run-up or inundation heights is governed by many factors of various space scales. The gross regional distribution of tsunami heights is considered to be determined by the characteristics of the tsunami source geometry dictated by a fault model of earthquake, together with the depth of water at the source area, orientation and distance of the fault plane relative to the coastline. Therefore, to improve our long-term predictive ability of tsunamis in this phase, it is essential to understand the space and time distribution of different kinds of fault mechanisms of large earthquakes in relation to global plate tectonics, the modes of subduction and/or collision of plates in particular.

This gross pattern of height distribution is, in reality, modified during tsunami propagation by various hydrodynamical factors such as wave refraction, diffraction, scattering and resonance due to topographic irregularities of various scales. The shape and bottom slope of the continental shelf, coastal indentation of large scale such as peninsulas, island-chains, submarine ridges are all relevant in this modification, and this is the phase where various kinds of hydrodynamical numerical model of tsunami exhibit their skill.

Furthermore, in the vicinity of a coastline, much finer details of the configuration of a shoreline and the immediate offshore topography, as well as the presence of breakwaters, seawalls, buildings and other obstructions on land, the terrain slope and the degree of roughness come into play in the determination of the local pattern of tsunami run-up, and, very often, non-linear and dispersive effects of waves and energy dissipation mechanisms are essential ingredients to be taken into account. The advance of technique to simulate a real tsunami by numerical means is quite significant, but the model used currently is relatively simple and has its limitation on the resolving power of phenomena near the shoreline and on land, beside the uncertainly related to the tsunami source model itself.

In this circumstance, it seems to be quite important to introduce a probabilistic description in space for tsunami warning practice and also for establishment of design criteria for engineering purpose, by taking the spacial variabilities of heights in local as well as regional scales into consideration.

References

1. Abe, Katsuyuki, "Quantification of major earthquake tsunamis of the Japan Sea," Phys. Earth Planet. Inter., 38, 214-223, (1985).

2. Aida, I., "A source model of the tsunami accmpanying the 1983 Nihonkai-Chubu earthquake," Bull. Earthq. Res. Inst., 59, 93-104, (1984). (J)

3. Akita Prefecture, "Survey of tsunami behaviours of the 1983 Nihonkai-Chubu earthquake along the coast of Akita Prefecture," Public Works Division, Akita Prefecture, 63p. (1984).(J)

4. ESTE(N. Shuto), "Report on the 1983 Nihonkai-Chubu earthquake tsunami," Bull. Experimental Station for Tsunami Engineering, Tohoku Univ., 1, 267p, (1984).(J)

5. Hatori. T., "Tsunami magnitude and source area of the Nihonkai-Chube earthquake in 1983," Bull. Earthq. Res. Inst., 58, 723-734, (1983). (J)

6. Japan Met. Agency, "Report on the Nihonkai-Chubu earthquake, 1983," Tech. Rep. Japan Met. Agency, No.106, 253p, (1984). (J)

7. Kajiura, K., "Tsunami energy in relation to parameters of the earthquake fault model," Bull. Earthq. Res. Inst., 56, 415-440, (1981).

8. Kajiura, K., "Some statistics related to observed tsunami heights along the coast of Japan," In Tsunamis - Their Science and Engineering, (Tsunami Symposium 1981) edited by K. Iida and T. Iwasaki, Terra Sci. Pub. Co., Tokyo, 131-145, (1983).

9. Noritomi, K.(editor), "General investigation on disasters caused by the 1983 Nihonkai-Chubu earthquake," Special Project Report on Natural Disasters, Ministry of Education, Science and Culture, No.58022002, 386p, (1984). (J)

10. NRCDP(Y. Tsuji, et al.), "Survey sheets of the heights of the tsunami caused by Nihonkai-Chubu earthquake," Review of Res. for Disaster Prevention, Nat. Res. Center for Disaster Prevention, 87, 306p, (1984). (J)

11. PHTRI(K. Tanimoto, et al.), "Field and laboratory investigations of the tsunami caused by 1983 Nihonkai-Chubu earthquake," Tech. Note, Port and Harbour Res. Inst., Ministry of Transport, No.470, 299p, (1983). (J)

12. PWRI(T. Uda), "Report on the disaster caused by the Nihonkai-Chubu earthquake of 1983 ; Tsunami, 17-54, and Damages of river structures and shore protection facilities by the tsunami, 209-230," Rep. Public Works Res. Inst., Ministry of Construction, No.165, (1985). (J)

13. Satake, K., "The mechanism of the 1983 Nihonkai-Chubu earthquake as inferred from long-period surface waves and tsunamis," Phys. Earth Planet. Inter., 37, 249-260, (1985).

14. Shuto, N., "The Nihonkai-Chubu earthquake tsunami on the north Akita coast," Proc. 31st Japan Conf. Coast. Eng., 247-251, (1984). (J)

15. Tsuji, Y., W.S. Baek, K.S. Chu and H.S. An, "Report of the 1983 Nihonkai- Chubu earthquake tsunami along the coast of the Republic of Korea," Review of Res. for Disaster Prevention, Nat. Res. Center for Disaster Prevention, 90, 96p, (1985). (J)

Table 1. Summary of observed tsunami heights, for the 1983 Japan Sea (Nihonkai-Chubu) Earthquake (M7.7; Mw7.9)

Segment Number	ID	Number of Samples		Average Height	Log Std. Dev.	Stand. Dev.	Extreme	Height
		N	N*	H_n	SD_n	$SD(H/H_n)$	H_{max}	H_{min}
1	I	26	23	0.64	0.246	1.76	1.92	0.20
2		4	3	0.33	0.226	1.68	0.50	0.16
3		4	2	0.35	0.039	1.09	0.50	0.21
4	I	4	4	0.49	0.228	1.69	0.70	0.20
5		5	3	0.71	0.057	1.14	1.00	0.55
6		6	4	0.48	0.149	1.41	0.90	0.19
7		7	5	0.73	0.158	1.44	1.10	0.40
8		2	1	0.24	0.0	1.00	0.30	0.20
9		4	3	0.64	0.146	1.40	1.56	0.40
10		20	12	1.10	0.195	1.57	3.17	0.30
11		11	5	0.68	0.426	2.67	10.50	0.10
12		14	7	1.14	0.095	1.24	1.50	0.60
13		16	7	1.40	0.087	1.22	2.15	0.70
14		19	8	1.57	0.090	1.23	2.70	1.19
15		21	10	1.41	0.104	1.27	1.95	0.80
16	I	80	25	2.82	0.218	1.65	6.95	0.90
17		26	13	2.30	0.128	1.34	4.10	0.80
18	I	3	1	3.35	0.0	1.00	3.80	3.00
19	P	18	8	1.18	0.114	1.30	3.70	0.70
20	P	6	5	0.48	0.121	1.32	0.70	0.35
21	P	3	3	0.51	0.086	1.22	0.65	0.40
22	P	1	1	0.42	0.0	1.00	0.42	0.42
23	P	1	1	0.42	0.0	1.00	0.42	0.42
24	P	1	1	0.52	0.0	1.00	0.52	0.52
25	P	1	1	0.44	0.0	1.00	0.44	0.44
26	P	2	2	0.35	0.018	1.04	0.37	0.34
27	P	2	2	0.48	0.018	1.04	0.50	0.46
28	P	1	1	0.40	0.0	1.00	0.40	0.40
29	P	3	3	0.19	0.383	2.42	0.65	0.0
30	P	2	2	0.37	0.565	3.67	1.35	0.0
31	p	0	0					
32	P	1	1	0.0	0.0	1.00	0.0	0.0
33		50	19	1.64	0.279	1.90	5.59	0.20
34		49	13	2.85	0.085	1.22	7.10	1.50
35		78	24	4.05	0.078	1.20	6.70	1.99
36		154	35	7.50	0.133	1.36	13.75	2.30
37		131	38	2.90	0.245	1.76	7.20	0.58
38		39	9	2.49	0.144	1.39	6.17	0.80
39		33	11	1.66	0.066	1.16	3.15	0.60
40	I	4	4	1.43	0.171	1.48	2.80	1.03
41		44	16	1.39	0.175	1.50	2.77	0.67
42		36	18	1.27	0.150	1.41	2.84	0.50
43	I	17	10	1.75	0.237	1.72	5.00	0.93
44A	I	17	12	0.90	0.209	1.62	2.00	0.43
45	I	11	9	0.74	0.133	1.36	1.40	0.50
44B	I	16	12	0.73	0.223	1.67	1.70	0.23
46	I	16	15	1.54	0.183	1.52	3.28	1.00

Table 1. Continued

Segment Number	ID	Number of Samples		Average Height	Log Std. Dev.	Stand. Dev.	Extreme	Height
		N	N*	H_n	SD_n	$SD(H/H_n)$	H_{max}	H_{min}
47		16	11	1.54	0.102	1.27	2.38	1.00
48		31	3	1.77	0.030	1.07	2.24	1.26
49		19	4	1.26	0.155	1.43	2.00	0.76
50		7	4	0.75	0.126	1.34	1.40	0.56
51		3	3	0.72	0.113	1.30	0.88	0.50
52		4	2	0.75	0.194	1.56	1.18	0.40
53		4	4	0.36	0.330	2.14	0.70	0.0
54		10	10	0.31	0.310	2.04	0.85	0.0
55		15	14	0.25	0.199	1.58	0.52	0.10
56		30	18	0.58	0.315	2.06	2.50	0.20
57	I	4	1	2.20	0.0	1.00	5.00	1.50
58		11	5	1.09	0.124	1.33	2.30	0.75
59		17	14	1.16	0.198	1.58	2.50	0.45
60		8	6	0.71	0.176	1.50	1.30	0.40
61		3	3	0.31	0.163	1.45	0.50	0.20
62		9	7	0.57	0.154	1.42	1.20	0.30
63		23	16	0.63	0.143	1.39	1.50	0.30
64		8	7	0.51	0.117	1.31	0.80	0.30
65		13	13	0.52	0.267	1.85	1.00	0.0
66		12	8	0.99	0.269	1.86	2.50	0.34
67		8	8	0.76	0.161	1.45	1.00	0.30
68		9	6	1.02	0.204	1.60	1.70	0.50
69		5	4	0.74	0.109	1.28	1.00	0.50
70		5	4	0.74	0.064	1.16	1.00	0.60
71		10	7	0.58	0.160	1.45	1.20	0.30
72		18	14	1.10	0.239	1.74	3.00	0.40
73		7	7	1.08	0.177	1.50	1.84	0.52
74	I	22	17	1.25	0.206	1.61	2.80	0.50
75	I	14	12	1.26	0.188	1.54	2.80	0.60
76		4	3	0.97	0.133	1.36	1.45	0.60
77		3	3	0.36	0.059	1.15	0.40	0.30
78		5	3	0.61	0.054	1.13	0.72	0.50
79		4	4	0.73	0.232	1.71	1.20	0.30
80		6	6	0.21	0.186	1.53	0.40	0.0
81	I	23	23	0.20	0.349	2.23	1.16	0.0
82	I	2	2	0.0	0.0	1.00	0.0	0.0

Segment number is as shown in Fig.1 with the length of about 40Km, provided that No.44 is separated into the west(A) and east(B) regions. ID is the data identification: P is the Pacific coast data and I is the island data. The number N* is for the processed data which are used for averaging (logarithmic). The standard deviation SDn is for log H, and the standard deviation of H/Hn is 10**SDn. Extreme values are those of all observed data in the segment. Data source: ESTE(1984), JMA(1984), NRCDP(1984), PHTRI(1983).

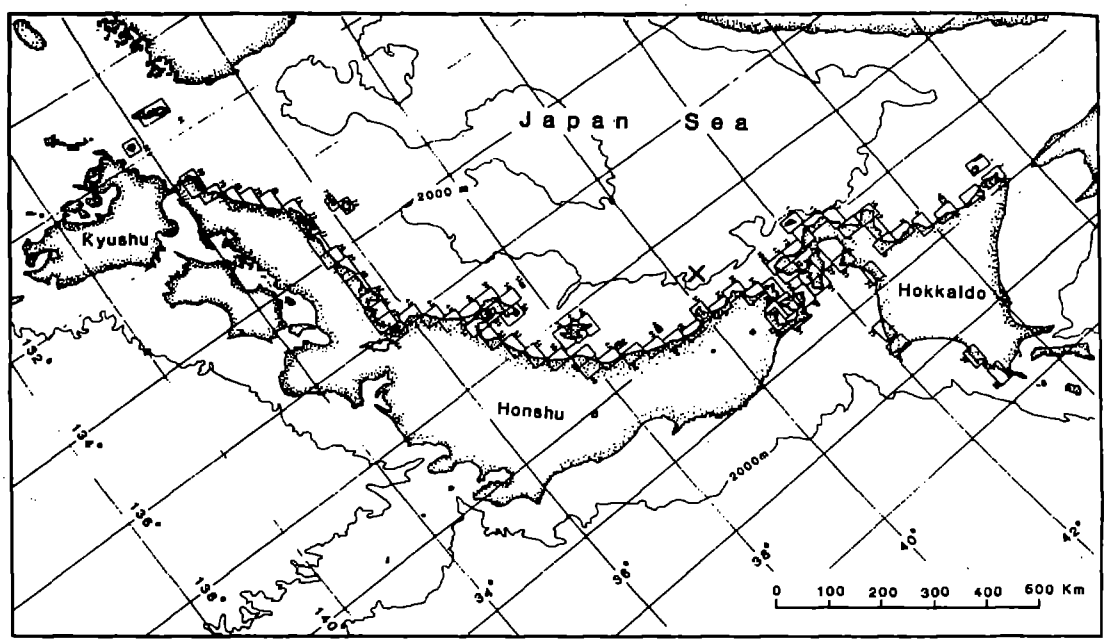

Fig. 1. Map showing the identification number of each segment, in which the averaging of runup data is made.

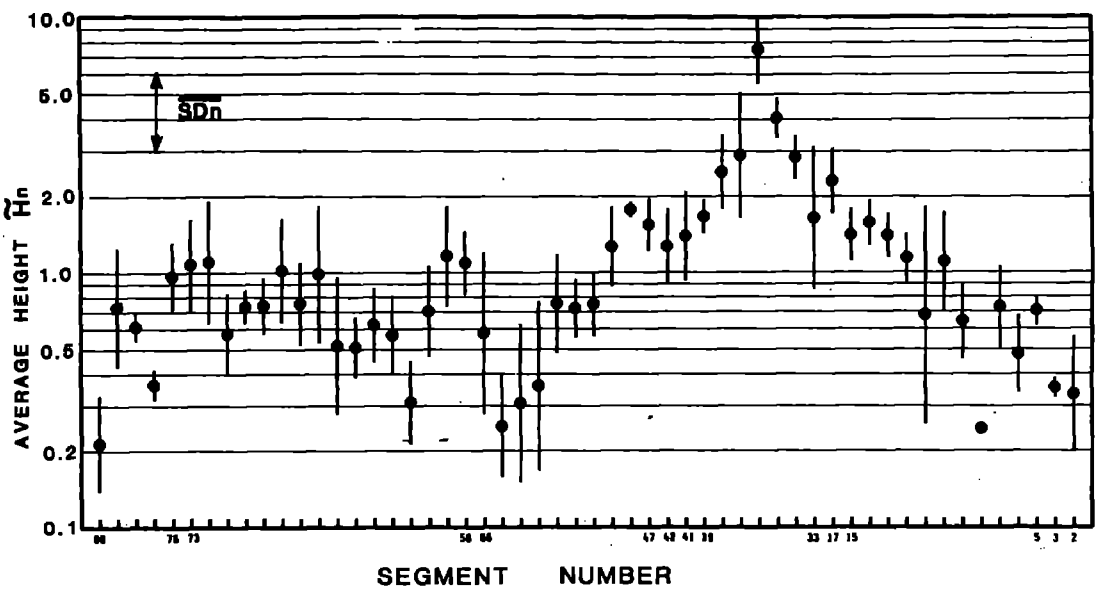

Fig. 2. Distribution of average runup heights Hn, together with their standard deviation SDn along the Japan Sea coast. Abscissa is in terms of the segment number shown in Fig.1. The segment numbers which are discontinuous along the coast are indicated.

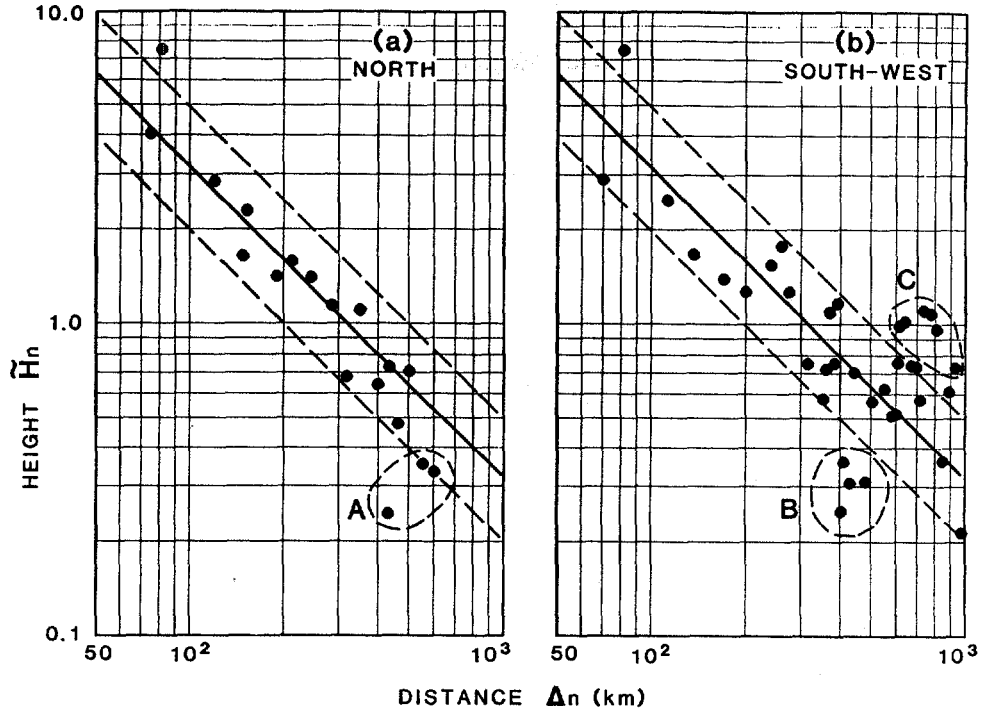

Fig. 3. Average Height Hn (m) as a function of distance Δn(Km) : [a] northern branch, [b] south-western branch. A thick line and broken lines are given by, Log Hn = - Log Δn + 2.50 ± 0.2.

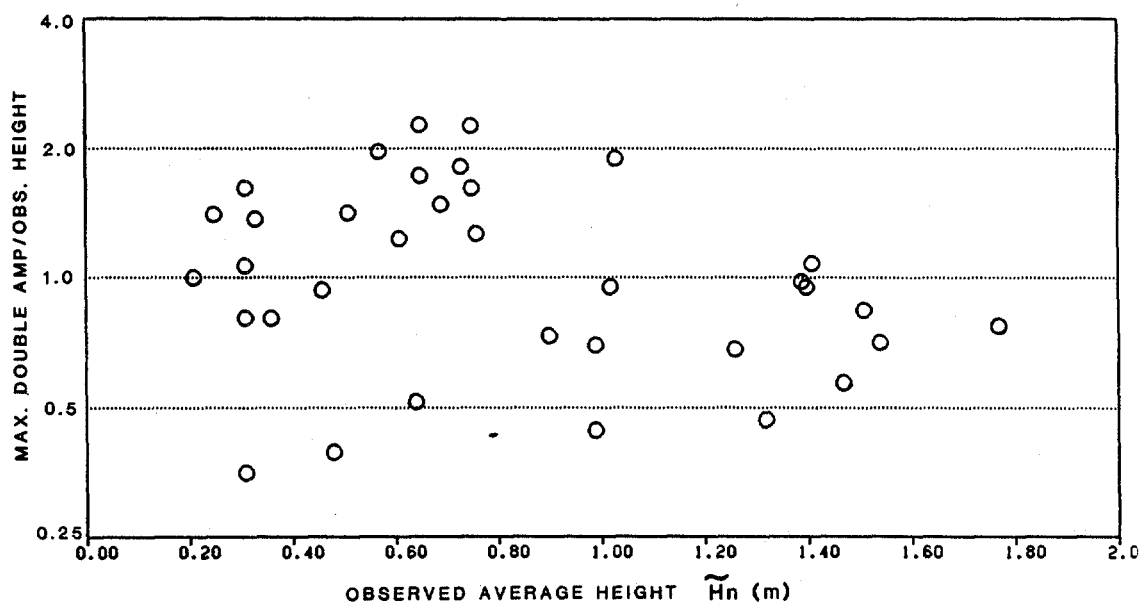

Fig. 4. Relation between the maximum double amplitude (crest to trough height) measured by the tide gauge and the average local runup height Hn .

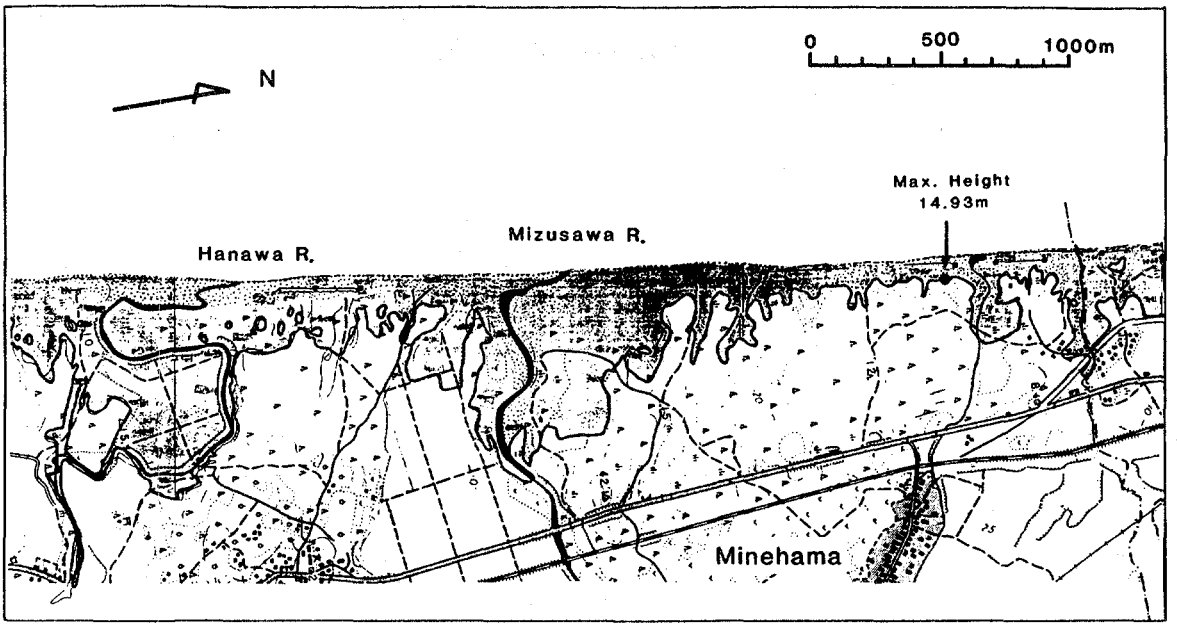

Fig. 5. Limit of tsunami runup on the Minehama coast in northern Akita Prefecture. Location of the maximum runup is shown by an arrow.

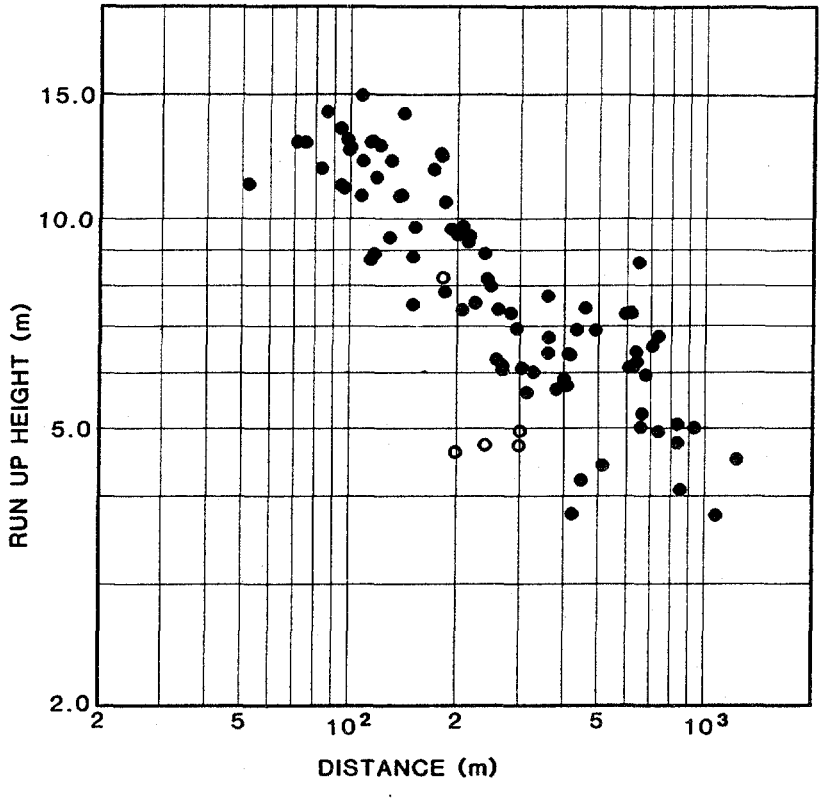

Fig. 6. Run-up height (m) as a function of the distance (m) from the shoreline on the Minehama coast (including Mizusawa R., Hanawa R. and Tako R. areas).

NUMERICAL SIMULATION OF THE TSUNAMI OF JUNE 23, 1946 IN BRITISH COLUMBIA, CANADA

T.S. MURTY AND P.B. CREAN
INSTITUTE OF OCEAN SCIENCES
DEPARTMENT OF FISHERIES AND OCEANS
P.O. BOX 6000
SIDNEY, B.C. CANADA V8L 4B2

ABSTRACT

On June 23, 1946 an earthquake with a magnitude of about 7.3 occurred on Vancouver Island in the Province of British Columbia, Canada. The epicenter was on land at 49.76°N, 125.34°W, but close to the shore. Associated with the earthquake, there was a vertical displacement in the land and ocean bottom of up to three meters. The resulting tsunami which killed one person and caused some damage was observed at several locations along the coastline. Here results of a numerical simulation of this tsunami are reported. A time-dependent two-dimensional numerical model was used which included the Strait of Georgia, and parts of the Johnstone and Juan de Fuca Straits. A radiation type condition was used at the open boundaries. The numerically simulated results on the amplitudes of the tsunami waves and the travel times are in good agreement with the few available observations.

1. INTRODUCTION

Rogers and Hasegawa (1978) studied the earthquake of June 23, 1946 in British Columbia, Canada. Figure 1 shows the geography of the Pacific coast of Canada and specifically, the Vancouver Island and Strait of Georgia areas where the earthquake occurred. The epicenter given by these authors was 49.76°N, 125.34°W and the surface wave magnitude was 7.2 ± 0.1. The epicenter was on Vancouver Island, close to its east coast.

According to Rogers and Hasegawa (1978) no major tsunami was created by this earthquake. However due to landslides and slumpings triggered by the earthquake, some minor water level disturbances occurred, and one person died.

In this study we numerically simulated the water level disturbances that occurred following this earthquake. As input into the numerical model we used the ground motion diagram (Figure 9c of Rogers and Hasegawa, 1978). In this diagram they showed vertical ground motion of up to 3 m, mostly on land but some in the Strait of Georgia. Surely, a subsidence of up to 3 m in a water body will likely generate a tsunami, even if it does not spread far and wide. Indeed our numerical simulation showed that there was no major Strait of Georgia-wide tsunami, but the water level disturbances were large enough to be noticeable, if not destructive.

2. THE NUMERICAL MODEL

The x-axis of a right-handed Cartesian coordinate system is taken along the length of the Strait of Georgia and the y-axis is taken along its width, with the origin being at the upper left corner (i.e. north-west corner). The grid size (Figure 2) in both directions is 2.62 km. There are a total of 91 grid points in the x-direction and 36 grid points in the y-direction.

The partly linearized shallow water equations are (the subscripts denote differentiation) (Henry, 1982; Murty, 1977, 1984):

$$\eta_t = -(du)_x - (dv)_y \qquad (1)$$

$$u_t = -g\eta_x + fv - F^{(u)} + G^{(u)} \qquad (2)$$

$$v_t = -g\eta_y - fu - F^{(v)} + G^{(v)} \qquad (3)$$

where

$\eta(x,y,t)$ = elevation of water surface above mean level
$u(x,y,t)$ = depth-averaged velocity in x-direction
$v(x,y,t)$ = depth-averaged velocity in y-direction
$d(x,y)$ = mean water depth
x,y = Cartesian coordinates in horizontal plane
f = Coriolis coefficient (assumed constant)
t = time

$F^{(u)}$ and $F^{(v)}$ represent friction terms. A quadratic bottom friction of the following form is used:

$$F^{(u)} = ku(u^2 + v^2)^{\frac{1}{2}}/d \; ; \; F^{(v)} = kv(u^2 + v^2)^{\frac{1}{2}}/d \qquad (4)$$

where k is a dimensionless bottom friction coefficient. The terms $G^{(u)}$ and $G^{(v)}$ in equations (1) - (3) represent forcing terms, such as surface wind stress, equilibrium tide gradient, etc., which may vary with x,y,t. For storm surge computations, these terms will represent the meteorological forcing terms and for tidal computations, they represent the tidal potential. For the present problem of tsunami generation and propagation, these terms are ignored and the forcing comes in the form of an increasing water level directly above the bottom (of the estuary) displacement.

A simple Richardson grid (Figure 3) was chosen as the basis for the finite-difference scheme on the grounds that it minimizes storage and permits particularly simple representation of coastlines. At interior points of the grid, equations (1) to (3) are represented by the following finite-difference forms:

$$\frac{\eta'_{ij} - \eta_{ij}}{\Delta t} = - \frac{(d_{ij} + d_{i+1,j})u_{j+1,j} - (d_{i-1,j} + d_{ij})u_{ij}}{2 \cdot \Delta x} - \frac{(d_{ij} + d_{i,j+1})v_{i,j+1} - (d_{i,j-1} + d_{ij})v_{ij}}{2 \cdot \Delta y} \quad (5)$$

$$\frac{u'_{ij} - u_{ij}}{\Delta t} = - g \frac{\eta'_{ij} - \eta'_{i-1,j}}{\Delta x} + f\tilde{v}_{ij} - F^{(u)}_{ij} + G^{(u)}_{ij} \quad (6)$$

$$\frac{v'_{ij} - v_{ij}}{\Delta t} = - g \frac{\eta'_{ij} - \eta'_{i,j-1}}{\Delta y} - f\tilde{u}'_{ij} - F^{(v)}_{ij} + G^{(v)}_{ij} \quad (7)$$

where

Δt = time step
$\Delta x, \Delta y$ = grid interval sizes in x,y directions respectively
d_{ij} = mean water depth at elevation points η_{ij}

$$\tilde{u}_{ij} = \frac{1}{4} u_{i,j-1} + u_{i+1,j-1} + u_{ij} + u_{i+1,j} \quad (8)$$

$$\tilde{v}_{ij} = \frac{1}{4} v_{i-1,j} + v_{ij} + v_{i-1,j+1} + v_{i,j+1} \quad (9)$$

Primes indicate variables updated during the current time step; unprimed variables are those evaluated at the previous step. The use of old (unprimed) values of v in the Coriolis term in (6) and new (primed) values of u in the corresponding term in (7) is necessary for stability. Fortunately, it also eliminates the need to store any but the most recently updated values of each variable, provided that the equations are applied in the order given, that is, at each time step, all the η_{ij} are updated, then all the u_{ij}, and finally all the v_{ij}. The same stability and storage conclusions apply if variables are evaluated in the

order η, v, u, using old values of u in the v-equation and new values of v in the u-equation. To reduce possible bias, the stepping subroutines evaluate the variables in the order η', u', v', on odd-numbered steps and η', v', u', on even-numbered steps.

Strictly speaking, equations (5) - (7) imply that u_{ij} and v_{ij} are evaluated $\Delta t/2$ later than η_{ij}, but normally they are regarded as pertaining to the same time level. The distinction is important only when calculating quantities which depend on phase differences between elevation and velocity, for example, energy flux, and then only when there are relatively few time steps per wave period.

A choice of a time step of 30 seconds satisfies the following stability criterion.

$$\Delta t \leq \left[g d_{max} \frac{\Delta x \cdot \Delta y}{(\Delta x^2 + \Delta y^2)} \right]^{\frac{1}{2}} \qquad (10)$$

where d_{max} is the maximum depth in the computational region.

Where there are good grounds for assuming that no waves enter the model area from an adjacent water body, it is appropriate to use a radiation condition on the sea boundary between the two. This permits waves reaching the sea boundary from the interior of the model to pass out of the model domain (Henry, 1982).

When choosing the model grid initially, radiating sea boundaries parallel to the x-axis of the model should be placed to run through v-points on the grid. Similarly, those parallel to the y-axis should run through u-points. It is assumed that the radiation problem can be treated one-dimensionally at each velocity point on the sea boundary and thus that the surface elevation and normal velocity at the boundary are related by

$$\text{outward normal velocity} = (g/d)^{\frac{1}{2}} \times \text{elevation}$$

Since there are no elevation points actually on the boundary, the nearest interior elevation value is taken instead, so that the formulas used in the stepping subroutines for u-points on radiating boundaries facing in the positive or negative x-direction are respectively:

$$u_{ij} = (g/d_{i-1,j})^{\frac{1}{2}} \cdot \eta_{i-1,j}$$

or

$$u_{ij} = - (g/d_{ij})^{\frac{1}{2}} \cdot \eta_{ij}$$

Similarly, at radiating sea boundaries facing in the positive or negative y-directions, the formulas used are respectively:

$$v_{ij} = (g/d_{i,j-1})^{\frac{1}{2}} \cdot \eta_{i,j-1}$$

or

$$v_{ij} = -(g/d_{ij})^{\frac{1}{2}} \cdot \eta_{ij}$$

When this type of radiation boundary condition is used, the permissible time step may be reduced by 50%. Hence, in the stability criterion (10) the denominator should be multiplied by a factor of 2.

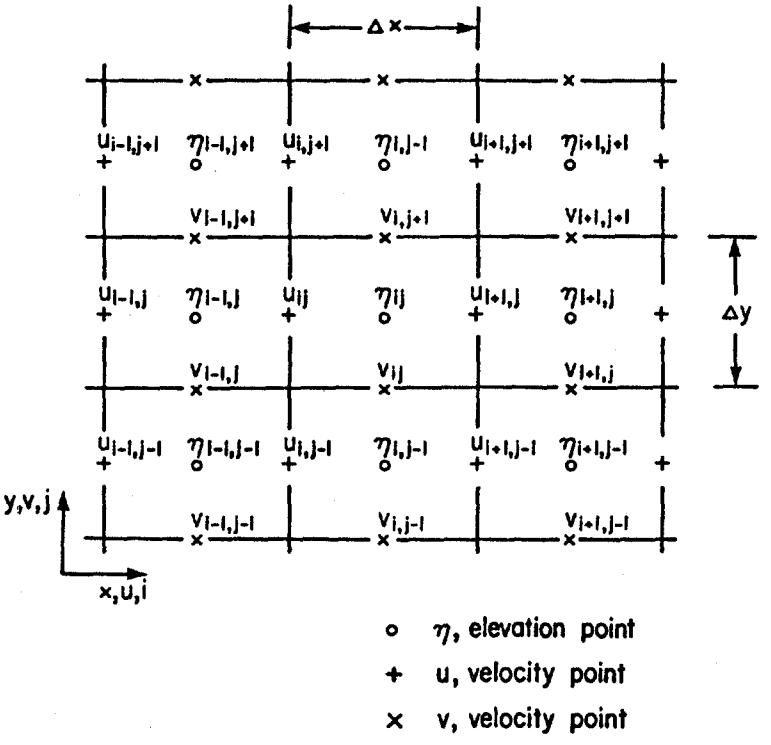

FIGURE 3. Computational scheme on the Richardson grid.

3. DISCUSSION OF RESULTS

The vertical ground displacement of up to 3 m as suggested by Rogers and Hasegawa (1978) was prescribed as the initial condition. Actually a mound of water 1 to 3 m high was prescribed initially in the area designated in Rogers and Hasegawa's paper and the numerical simulation involved propagation of this initial elevation (mound of water). As expected, the tsunami did not propagate Strait of Georgia-wide with significant amplitudes.

Figures 4a and b show the time series of the computed water levels at various locations along the west and east shores of the Strait of Georgia including some islands. Table 1 lists the approximate range of the water level associated with the tsunami at these locations. From Figures 4a and b and Table 1 the following important results can be deduced. Some areas farther from the initial ground subsidence associated with the earthquake have greater tsunami range than areas closer. This is mainly due to damping of the tsunami waves in shallow areas and amplification in some inlets due to resonance.

In particular, we first will examine the tsunami range along the western shores of the Strait of Georgia. Even though Comox is farther than Campbell River, the tsunami range was greater at Comox. A similar situation exists with reference to Parksville and Nanaimo. Even though Parksville is closer to the epicenter than Nanaimo, the tsunami amplitude at Parksville is somewhat smaller because the extensive shallows and tidal flats at Parksville damped the tsunami waves significantly. The tsunami amplitudes at Galiano and Orcas Islands were also small due to damping and absence of resonance effects.

Next directing our attention to the east shore of the Strait of Georgia, some amplification of the tsunami in Howe Sound and Burrard Inlet is noticeable. Also associated with this tsunami, a regular seiche occurred in Jarvis Inlet. It would have been better if comparisons could be made between these computer water levels and water levels recorded on tide gauges. Rogers and Hasegawa (1978) mentioned that the Vancouver and Victoria tide gauges showed no tsunami.

In conclusion, the computed water levels shown in Figure 4 and Table 1 are unverified against any observations. It is not claimed here that these water levels necessarily occurred; rather it is shown that, if the vertical ground motion as given in Figure 9c of Rogers and Hasegawa (1978) has occurred, then a small tsunami would have occurred in the Strait of Georgia.

TABLE 1

Approximate range of the tsunami (m) at several locations in the Strait of Georgia, associated with the June 23, 1946 earthquake. The locations are listed from north to south separately for the western and eastern shores of the Strait

Locations along the west shore	Tsunami range	Locations along the east shore	Tsunami range
Quadra Island	-0.5 to 1.2	Sutil Channel	-0.4 to 1.0
Campbell River	-0.9 to 1.4	Powell River	-0.8 to 1.0
Comox	-1.3 to 1.4	Jarvis Inlet	-0.4 to 0.4
Parksville	-0.2 to 0.3	Sechelt	-0.3 to 0.4
Nanaimo	-0.9 to 0.9	Howe Sound	-0.9 to 0.9
Galiano Island	-0.2 to 0.2	Vancouver (Burrard Inlet)	-0.8 to 0.7
Orcas Island	-0.1 to 0.2	White Rock	-0.4 to 0.4

ACKNOWLEDGEMENTS·

We thank Billie Mathias for typing the manuscript and Ms. Coralie Wallace for drafting the figures.

REFERENCES

Henry, R.F. 1982. Automated programming of explicit shallow-water models: Part I. Linearized models with linear or quadratic friction, Can. Tech. Rep. Hydrogr. Ocean Sci. No. 3. Institute of Ocean Sciences, Dept. of Fisheries and Oceans, Sidney, B.C., Canada. 70 pp.

Murty, T.S. 1977. Seismic sea waves - tsunamis. Bull. No. 198, Fish. Res. Bd. Can., Ottawa. 337 pp.

Murty, T.S. 1984. Storm surges - meteorological ocean tides. Bull, No. 212. Can. Bull. Fisheries and Aquatic Sciences, Ottawa. 906 pp.

Rogers, G.C. and H.S. Hasegawa. 1978. A second look at the British Columbia earthquake of June 23, 1946. Bull. Seismological Soc. America, Vol. 678, No. 3, 653-676.

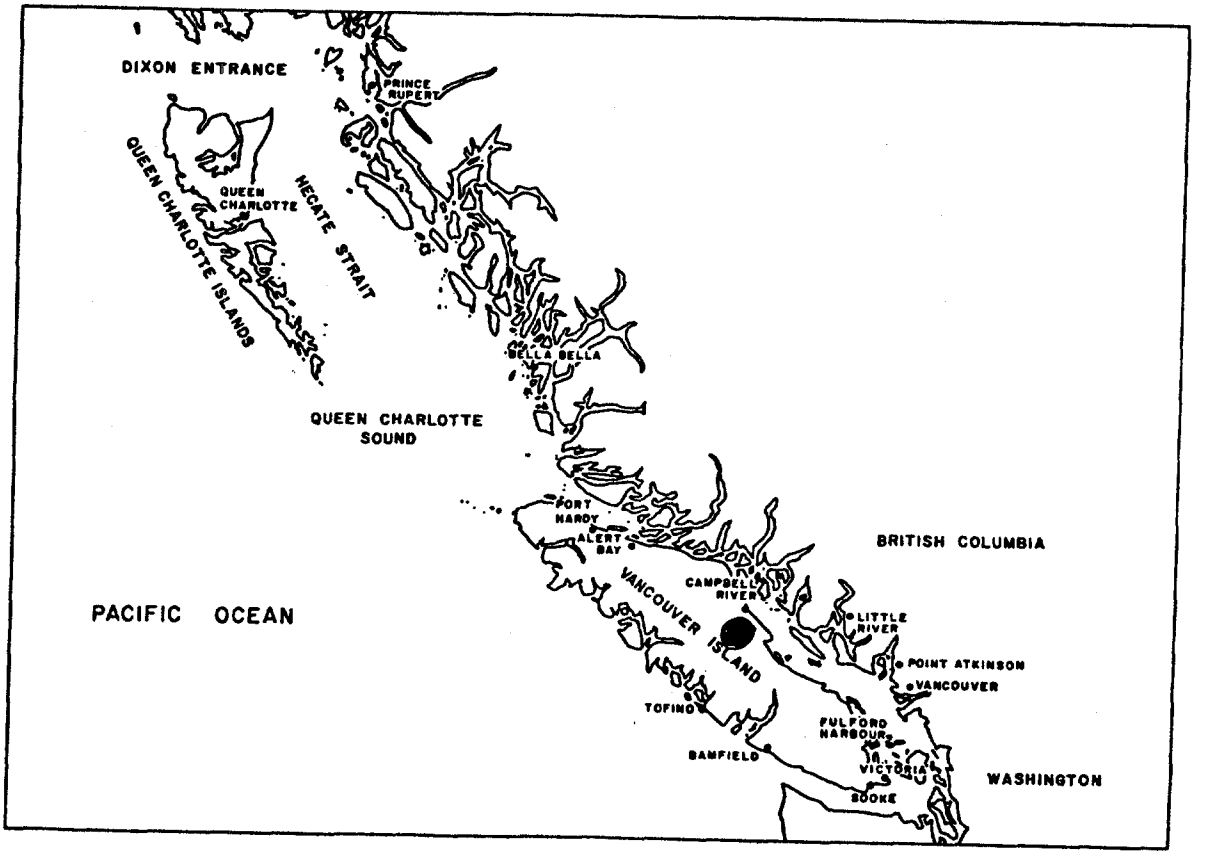

Figure 1. A geographical map of the southern part of Pacific coast of Canada, showing Vancouver Island and Strait of Georgia areas. Epicenter of the earthquake of June 23, 1946 is shown by a dark circle.

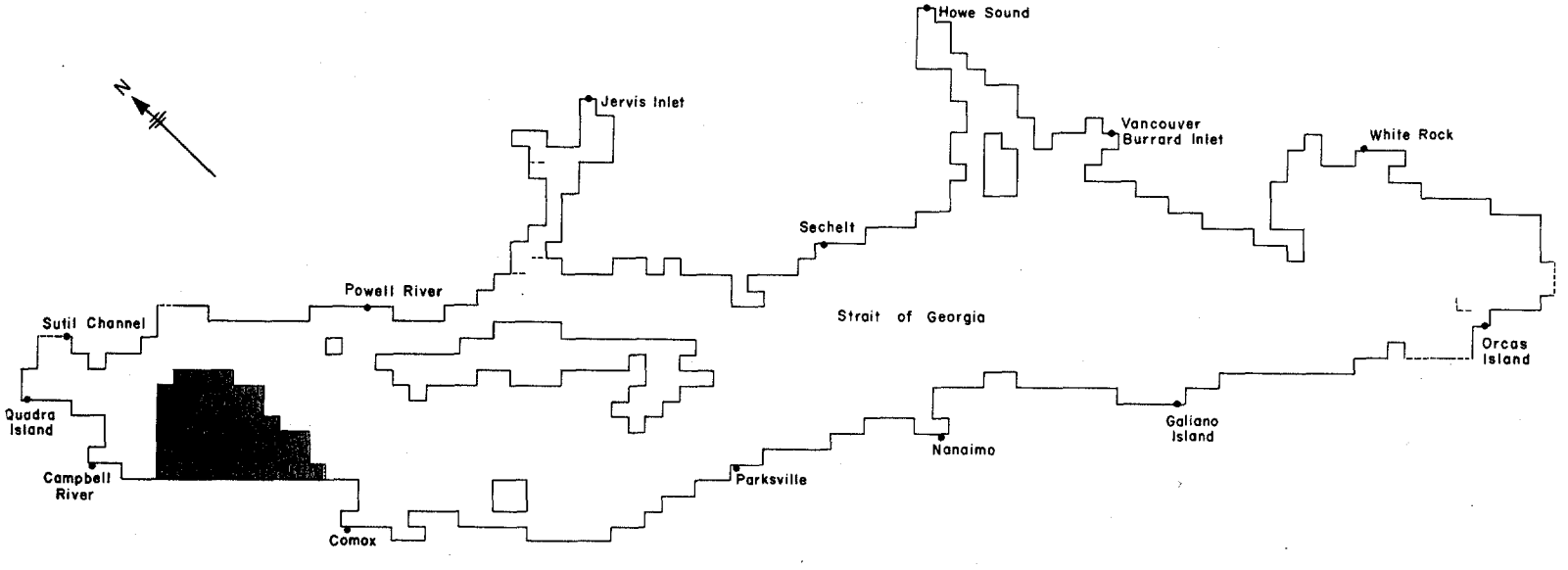

Figure 2. Grid used for numerical simulation of the tsunami. Various locations are shown at which the computed water level time series is given in subsequent figures.

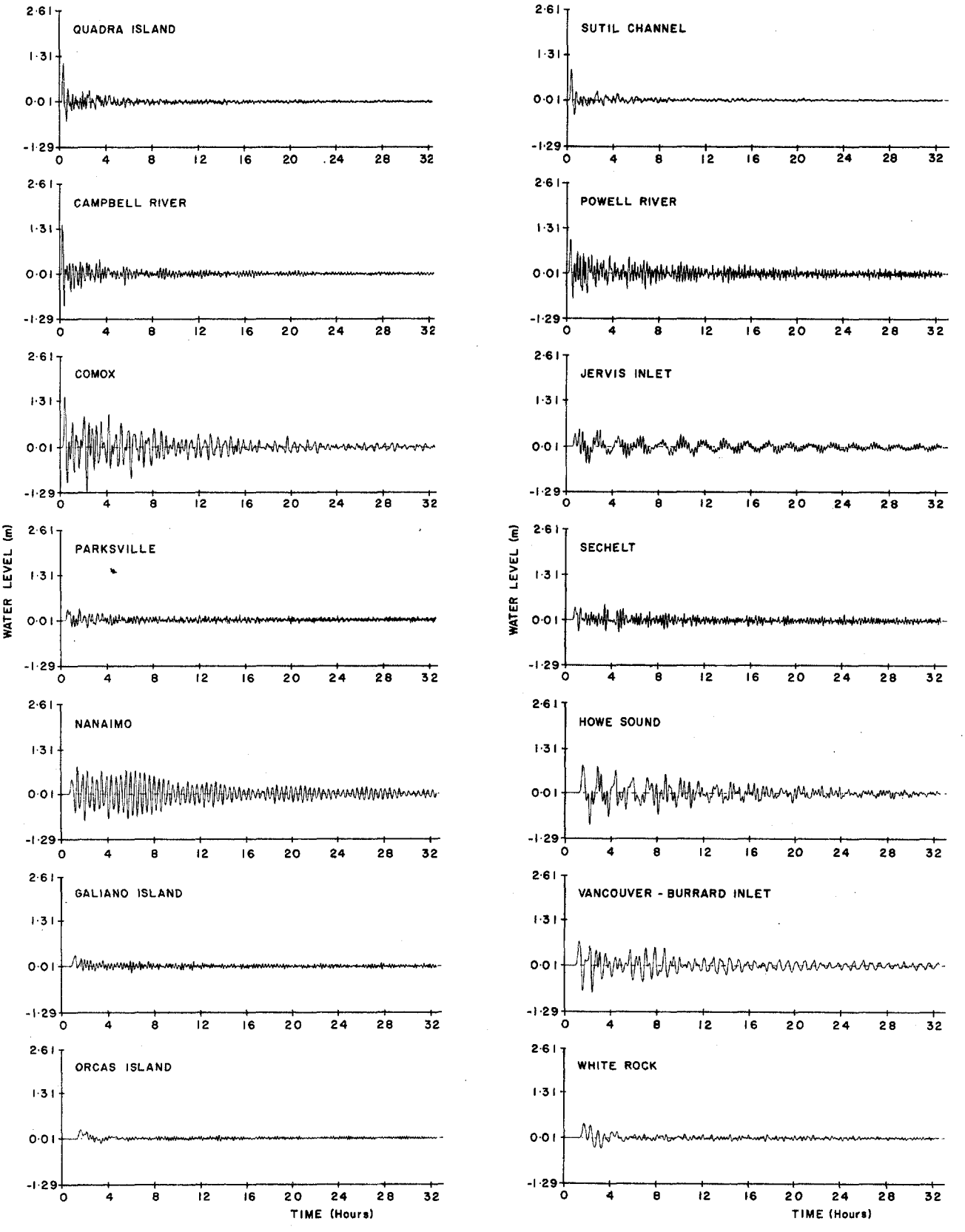

Figure 4. Computer water levels at several locations along the west and east shores of the Strait of Georgia, due to earthquake of June 23, 1946

WAVE FORCE OF TSUNAMI BORE ON A VERTICAL WALL

Hiroyoshi Togashi

Department of Civil Engineering, Faculty of Engineering, Nagasaki University, Japan

ABSTRACT

As regards wave force of tsunami bore acting on a structure, there are several problems left to be resolved. Above all, in a case where tsunami overflows some structure after colliding against it, the generation mechanism and the magnitude of dynamic wave force due to mean water particle velocity of tsunami bore reflected from the structure are not yet elucidated.

In the paper, the structure is treated as a vertical wall model simulating a tsunami protection gate against river run-up tsunami or a land dike protecting against land run-up tsunami. Profiles of wave height and cross-sectional mean velocity of both partial clapotis bore in front of wall and transmitted surge to rear of it are experimentally obtained, by which wave force of tsunami bore on a vertical wall is evaluated and mechanism of wave force is tried to make clear. As the result, it became evident that the dynamic wave force is mainly generated by drag force and the magnitude of it is some 10~40 % of static wave force.

I . INTRODUCTION

When some structures are broken down or flowed away by tsunami, one of the reason of which is considered to be due to wave force of tsunami acting directly on a structure, and such a tsunami would be a fairly big one of the magnitude.

The object of the present study is a tsunami bore such that becomes bore after breaking from near wave front in the sea, which runs against a tsunami protection gate in the case of river run-up or runs against a tsunami protection wall like land dike in the case of land run-up. And, the purpose of the study is experimentally to investigate the hydraulic mechanism of tsunami bore reflected from a vertical wall and the mechanism generating dynamic wave force on a vertical wall.

Incidentally, there are so far some investigations in relation to the dynamic wave forces of run-up tsunami on a structure[1),2),3),4)]. All of these, however, treated surge forces caused by the leading edge of the surge impinging on a structure, which are different from the treatment of the problem like wave forces of tsunami bore in the case where flow overtops the structure of finite height that becomes the object of this study.

In the study of Fukui et al[2)], tsunami overtopping a land dike was the object, so it looks like similar treatment to this study in appearance. However, hydrodynamic forces are presented by celerity of bore front of tsunami approaching shoreline, so that they all the same are considered as the surge forces. And, although the object of the study by Nakamura[4)] is tsunami protection gate, his study as well pays mainly attention to the surge forces comparing with the methods by Cumberbatch[1)] and Cross[3)], accordingly it is hardly referred to hydrodynamic forces of partial clapotis bore in cases with flow overtopping the gate or the vertical wall.

Therefore, the treatment of this study about tsunami bore, especially using mean velocity, would be the first trial as far as wave forces, not surge force, are concerned.

II. EXPERIMENTAL EQUIPMENTS AND PROCEDURES

The equipment consists of a wave generater of pneumatic type and a two dimensional wave flume of 1.0 m deep and 60.0 m long, in which a sloping bottom model of composite type beach is installed being combined with two kinds of sea bed slopes (S = 1/50, 1/20) and a river bed or land slope (S = 1/600) as shown in Fig.1. Wave gages are of capacitance type and current meters are of screw type of small size. Pressure gages of small size are set to the foreface of vertical wall. An incident wave profile at the toe of sea bed slope is non-periodic and analogous to a solitary wave, the shape of which is a kind of sinusoidal wave on a still water level.

An incident wave breaks like a surging breaker on the slope from near the end of the slope S = 1/50 to the slope S = 1/20, and it becomes the weak bore and reaches the shoreline.

An incident surge runs up with a violent velocity like a supercritical flow on a mild slope S = 1/600 near horizontal and runs against a vertical wall and finally overflows it.

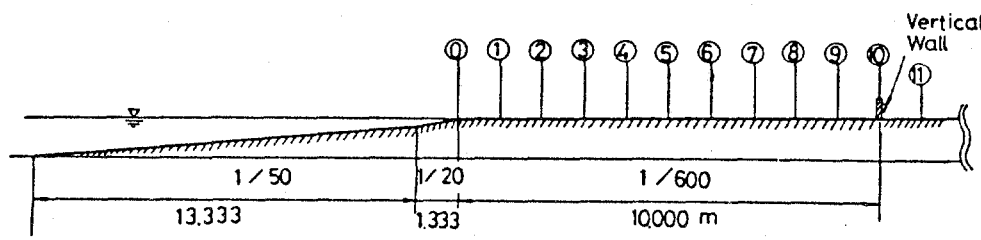

Fig. 1 Side view of experimental bed slopes

The point of the problem is the effect of an unsteady flow of wave overtopping on wave force and is how to successfully grasp velocity of reflected bore in front of a vertical wall. In order to investigate it, wave height, velocity in front of the vertical wall and wave pressure on the wall are necessary to be simultaneously measured. Therefore, measuring points were set at the wall site and several positions in front of the wall, where measured velocities were averaged vertically from several values of every 5 cm high in a section at any locations.

III. RESULTS AND DISCUSSIONS

According to the author's previous investigations regarding the case study on tsunami protection gate[5], the result was obtained that the maximum wave pressure of bore reflected from the flood gate was round 10 % larger than hydrostatic pressure at the site of the flood gate overflowing. The mechanism, however, generating the hydrodynamic pressure was not clarified. Therefore, the present experiment focuses on measuring velocity of reflected bore and investigating velocity contributing to generation of hydrodynamic pressure.

3.1 Wave profile of incident surge, reflected bore and transmitted surge

A side view of the experimental bed slopes is shown in Fig.1. A vertical wall model is installed at the position of 10.0 m landward from shoreline. Four kinds of wall heights H_d = 4, 8, 12 and 16 cm high were used, each of which corresponds to round 0.5, 1.0, 1.5 and 2.0 times as high as the maximum height $H_{i,max}$ of incident surge in the case with no wall at the wall site.

Figure 2 is an example of wave profiles of bore height and velocities with respect to time at the position of 10 cm just in front of the wall in the case of P-2 ($H_d \fallingdotseq H_{i,max}$) which is typical of construction design in

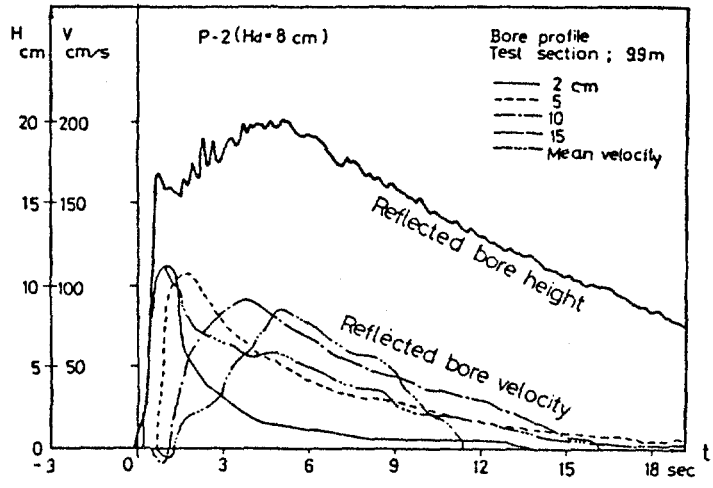

Fig. 2 An example of wave profiles of bore height and mean velocities

general. As the position is just in the foreface of the wall, the wave profiles are regarded as partial clapotis nearly at the wall site. A mean velocity in the section was obtained by averaging four points of values of 2, 5, 10 and 15 cm high above bottom. However, when the surge height is too small to touch the current meter, the mean velocity was obtained from velocities less than three points. In figures following after this, the origin of time t (= 0) is set at the moment when an incident surge front just arrived at the vertical wall.

Figures 3(a) and 3(b) too are in the same case as in Fig.2 of standard wall height ($H_d \fallingdotseq H_{i,max}$) which can be often seen as tsunami protection facilities today. Figure 3(a) shows wave heights only and Fig.3(b) shows velocities only, and the profiles at the several measuring points are shown superimposed in each of the figures. Each of the solid lines is the wave height or velocity of the incident surge at the measuring point ⑧ (2.0 m distant from the wall) in the case without wall. It is clearly evident from Figs.3(a) and 3(b) that, when an incident surge like this one were given as an input near at the wall, how wave profiles of bore reflected from the wall and transmitted surge to rear of it would be occured as outputs at each of the measuring points. Wave profiles of reflected bore heights and velocities are nearly analogous to one another and almost the same magnitude as in each of them after initial transient state in spite of any positions.

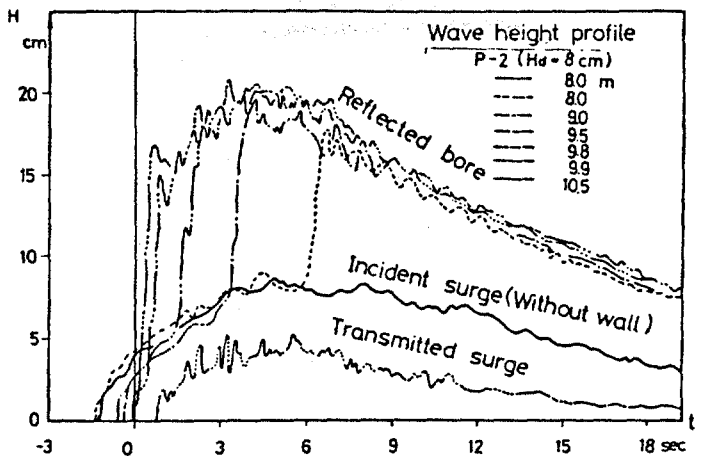

Fig. 3(a) Wave profiles of wave heights of bore and surge

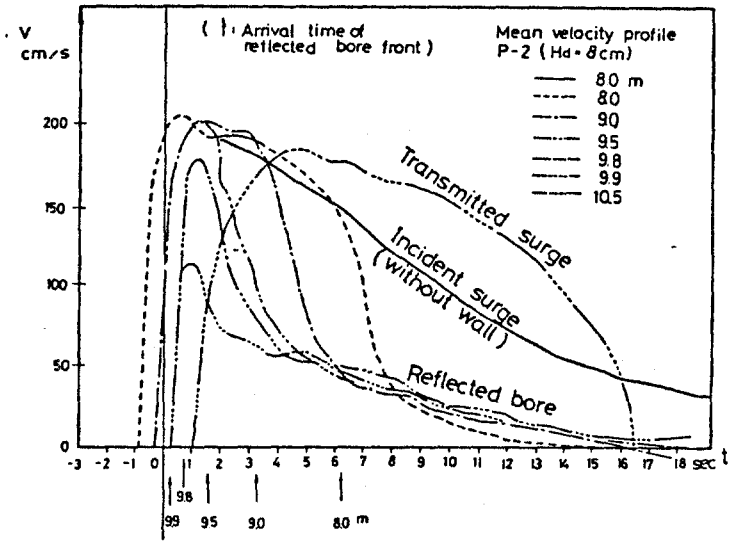

Fig. 3(b) Wave profiles of mean velocities of bore and surge

Although, according to Fig.3(a), bore height profiles are formed after about 1 sec from the instant when the shock front of reflected bore was appeared in the incident surge profile at each of the positions, the mean velocity profiles of bore shown in Fig.3(b) seem to be settled down at certain considerably stable velocity like bore after 2~3 sec from the arrival time of reflected bore front as shown by arrow marks below abscissa, so phase shift between bore height and velocity is clearly seen. This is very important to know exactly the position and time of velocity which would act dynamic wave force on the wall face. That is to say, it is about 6 sec for shock front to arrive at the measuring point ⑧, however the velocity of partial clapotis (bore) following shock front which seems to act dynamic wave force on the wall should be considered as velocity after 8 sec becoming nearly in agreement with velocities at the other positions. In other words, it could be considered that, at the time (t ≒ 6 sec) when shock front arrived at the position ⑧, the velocity of bore acting dynamic wave force on the wall is the one after 6 sec at the positions of 9.0, 9.5, 9.8 and 9.9 m closer to the wall. This is a standard of concept of how to evaluate velocity of partial clapotis in front of the wall.

Figure 4 shows difference of velocity changes of reflected bore when taking the wall heights as parameter at the position of 9.0 m specified as an example and in the figure the effect of the wall heights is evidently recognized, which results in the same way as at the other positions.

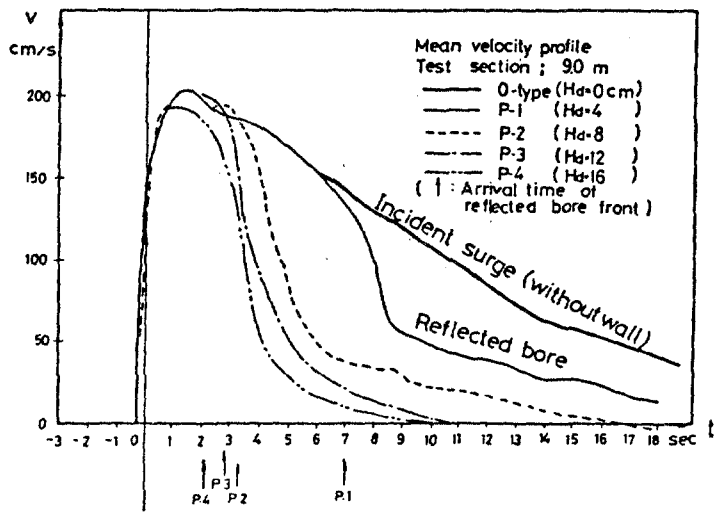

Fig. 4 Difference due to wall heights of mean velocity changes of reflected bore

According to the examples of Figs.3 and 4, in the case where the vertical wall site (10.0 m in the case) and the wall height are given, the reflected bore height and velocity in the case with wall is seen to be obtained from the incident surge height and velocity in the case without wall at certain position (8.0 m in the case) in front of the wall. Therefore, if this can theoretically be explained to some degree, that would be useful to clarify the hydraulic mechanism of the reflected bore and the generation of dynamic wave force on the wall.

3.2 Estimation of wave pofile of reflected bore and transmitted surge from incident surge by application of steady flow theory

Figure 5 is a schematic diagram of steady flow model used for analyzing a typical tsunami phenomenon colliding against a vertical wall like a land dike.

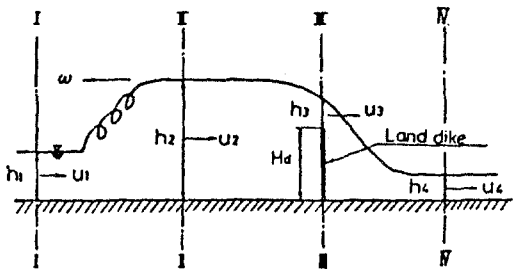

Fig. 5 Schematic diagram for analysis of tsunami phenomenon overflowing a vertical wall

As the method of analysis in this case was already presented by the authors[6], the results only are here shown. The points to be noted in Fig.5 are the section I giving an incident surge as an input, the section II giving reflected bore and the section IV giving transmitted surge as outputs. The calculated results are shown by the thin solid lines in Figs.7 through 9.

By the way, in Fig.6, the two bold solid lines are experimental curves of incident surge as an input at the position ⑧ in the case without wall.

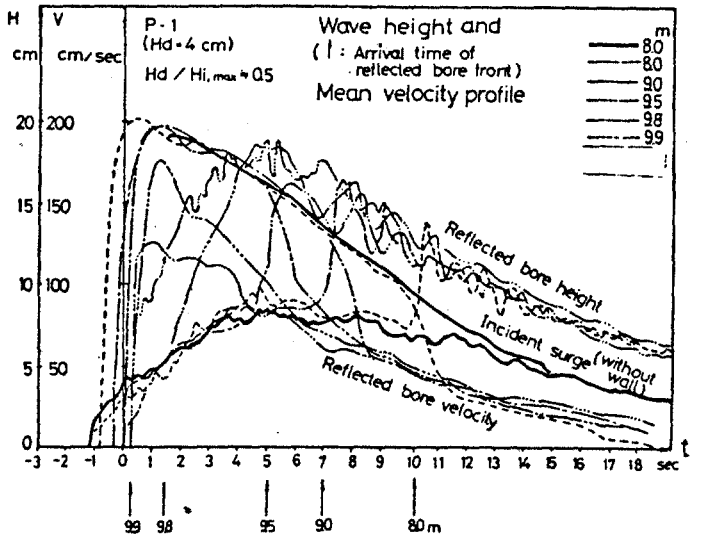

Fig. 6 Superposition of wave profiles of wave heights and mean velocities of incident surge and reflected bore

And, in a case where a wall with a certain height is installed at the position ⑩, wave profiles of reflected bore are experimentally obtained as shown by broken or chain lines as outputs at the positions between the points ⑧ and ⑩ in front of the wall, and the same thing is said of transmitted surge to rear of it.

In the same way as in the experiment, theoretical wave profiles by the theory mentioned before are simultaneosly obtained of both reflected bore and transmitted surge as outputs from the incident surge as an input at the position ⑧.

However, as the figure including the both wave heights and mean velocities like this is fairly complicated and hard to see, it seems to be better to divide them into two separate figures, so that each of them consists of wave heights or velocities only. Therefore, in Figs.7 through 9, figures are separately drawn and discussed in regard to wave heights and velocities.

In Figs.7(a), 7(a)′ and 7(b), the two thin solid lines are results computed theoretically from the incident surge shown with the thick solid line in the case of P-1. Applicable range of theory is for small interval from 7 to 12 sec. As the top of the wall is lower than the incident surge height as a whole, the surge easily overtops the wall presenting behaviour like a supercritical flow for initial several seconds and bore is not formed before 7 sec. And after 12 sec, the overtopping discharge becomes zero and perfect clapotis bore is formed theoretically, however in fact the wave heights of bore and surge gradually decrease, for which the theory is not covered.

Tendency of the computed results is not so good in agreement with the experimental results, but values near peak are roughly in agreement with the experimental ones. That could be understood by shifting the phase for about 1.5 or 3.0 sec as shown in Fig.7(a)′ .

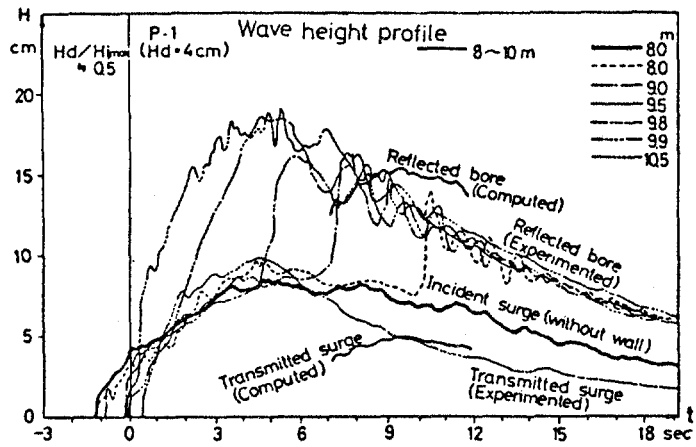

Fig. 7(a) Comparison of computed results with experimental wave heights in the case of P-1

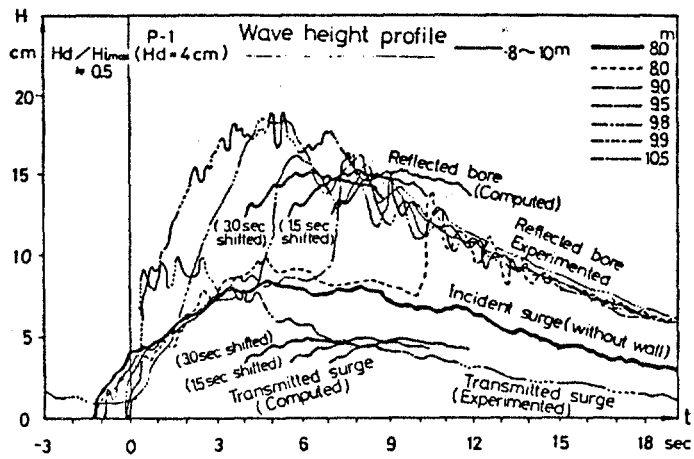

Fig. 7(a)' Comparison of computed results with experimental wave heights by phase shift in the case of P-1

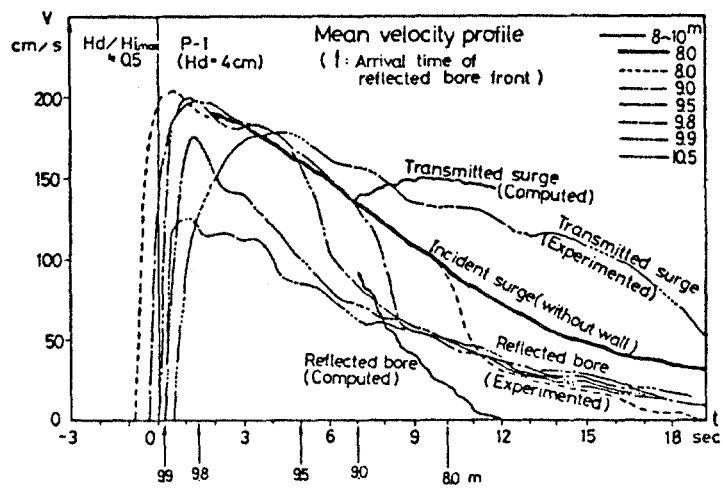

Fig. 7(b) Comparison of computed results with experimental velocities in the case of P-1

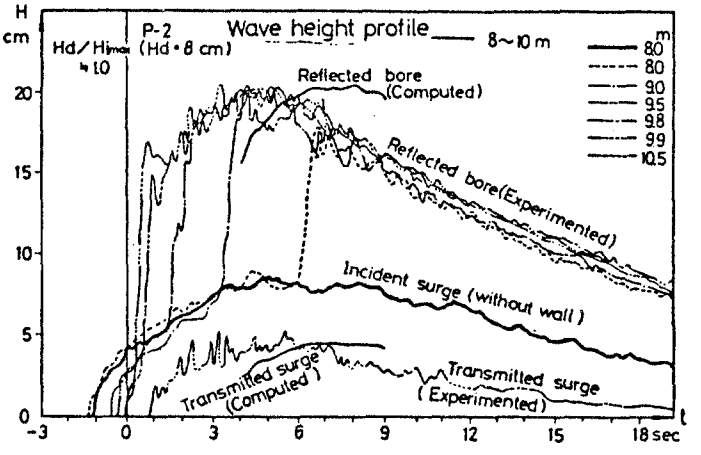

Fig. 8(a) Comparison of computed results with experimental wave heights in the case of P-2

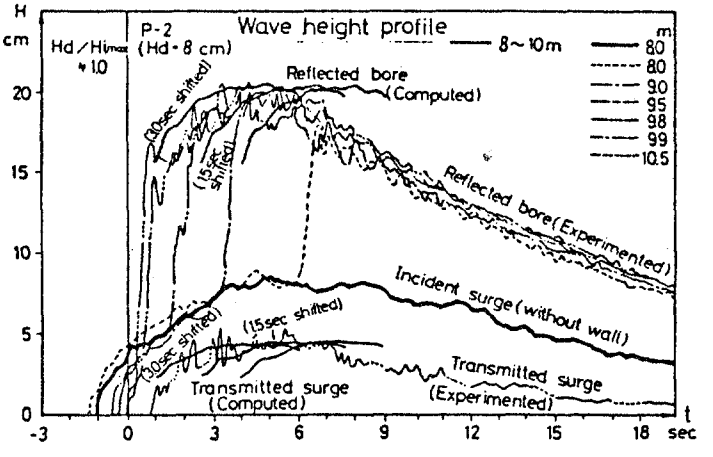

Fig. 8(a)' Comparison of computed results with experimental wave heights by phase shift in the case of P-2

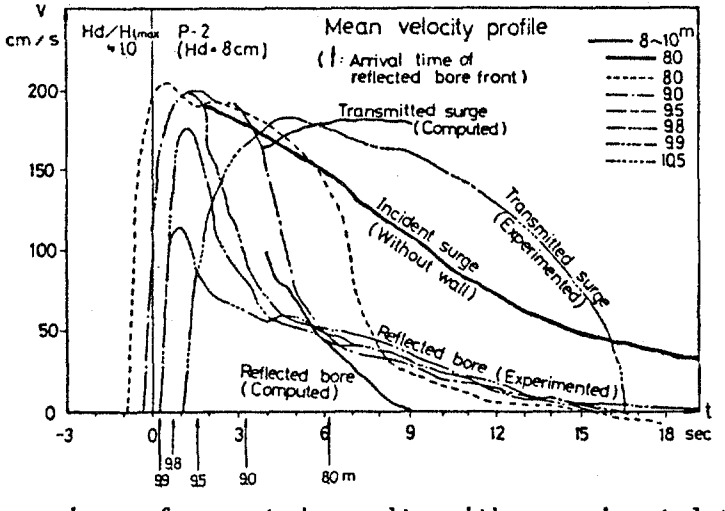

Fig. 8(b) Comparison of computed results with experimental velocities in the case of P-2

Figures 8(a), 8(a)' and 8(b) are in the case of P-2. Difference from P-1 is that applicable range appear in a little earlier time than P-1 as a whole and bore is formed near at 4 sec as shown in Figs.8(a) and 8(b). It means that the wall height is higher than P-1 and the reflected bore is easily formed. The whole tendency and values near peak are almost the same as in the case of P-1, however the computed results of which phase are shifted for 1.5 or 3.0 sec in Fig.8(a)' are fairly well in agreement with the experimental curves.

In Figs.9(a) and 9(b) in the case of P-3, the top of the wall is considerably high, so bore is nearly instantaneously formed just after when the incident surge front reached the wall. Agreement of the computed results with the experimental curves is good on the whole. Others are almost the same as in the cases of P-2 and P-1.

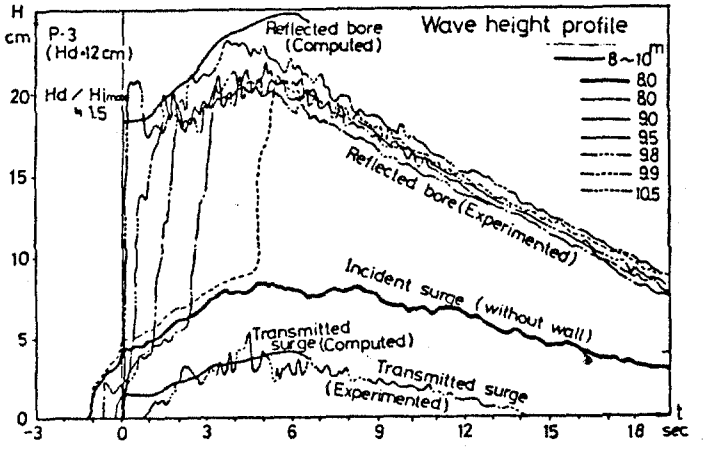

Fig. 9(a) Comparison of computed results with experimental wave heights in the case of P-3

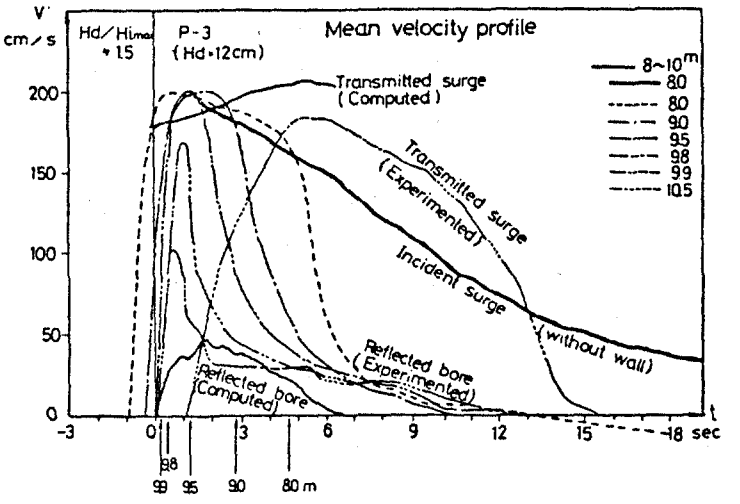

Fig. 9(b) Comparison of computed results with experimental velocities in the case of P-3

Therefore, according to Figs.7 through 9, if steady flow theory by the author is applied to wave height and velocity of both reflected bore in front of the vertical wall and transmitted surge to rear of it, the values near peak were seen to be roughly explained by the theory, although there is a little time lag affected by rising surge front portion.

This is very important thing to design some tsunami protection facility,

because the most tsunami protection facilities are designed based on the maximum inundation trace height of the past tsunamis.

3.3 Numerical estimation of dynamic wave force on the wall by observed velocity.

Two methods of estimation are here presented. One of them depends on successive computation of form drag by momentum change over the interval putting the wall between the both two sections for every time increment $\Delta t = 0.1$ sec as an example case shown in Fig.10. This method is comparatively

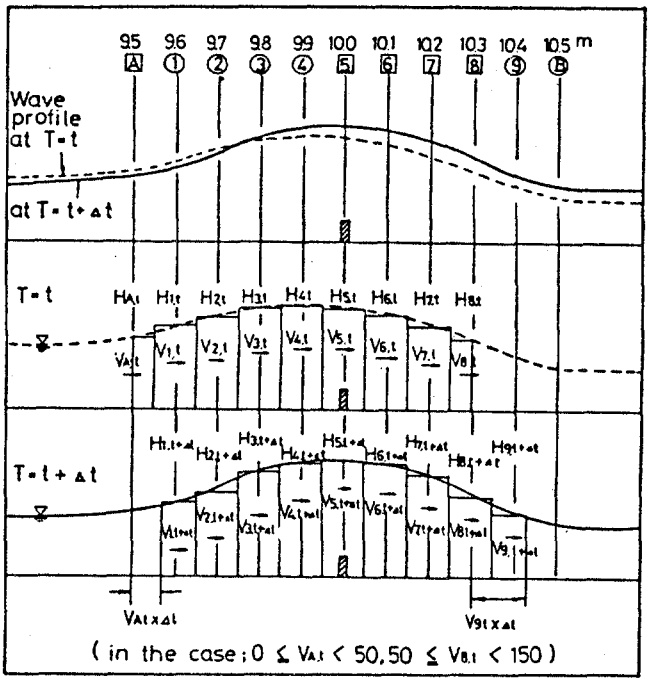

Fig.10 An example case showing how to compute form drag by momentum change

well applied only to the case of wave overtopping phenomenon like a supercritical flow as shown by the thick dotted line in Figs.11 or 12, and the computed results show qualitatively similar tendencies to the measured values, though the data are fairly scattered.

The nondimensional wave force p/wH on the left side of ordinate is the ratio of dynamic wave force pH_d to hydrostatic force wHH_d which are measured for the different wall height H_d in each of cases shown in Figs.11 through 14, where p is the dynamic wave perssure which the hydrostatic pressure wH is subtracted from the total wave pressure, each of which is the value averaged on the wall. And $w = \rho g$, where ρ is the density of water and g is gravitational acceleration.

The above description is referred in the same way to the nondimensional drag force $C_D U^2/2gH$ on the right side of ordinate as well.

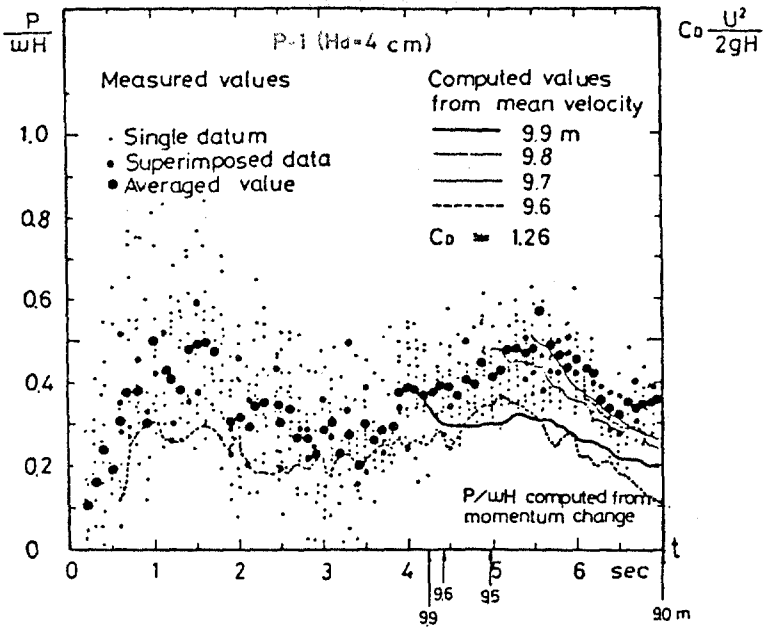

Fig.11 Comparison of computed drag forces with experimental dynamic wave forces in the case of P-1

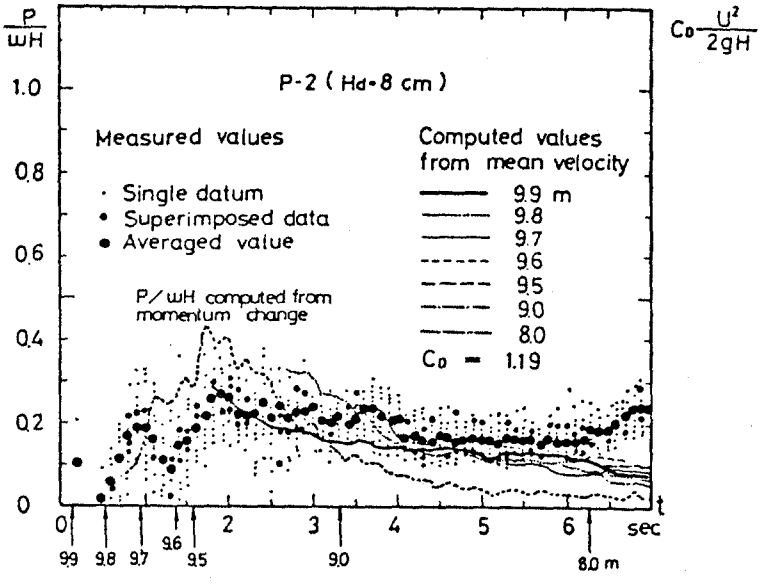

Fig.12 Comparison of computed drag forces with experimental dynamic wave forces in the case of P-2

Then, another method is evaluation by drag force calculated from mean velocity of reflected bore shown in Figs.11 through 14. Here, drag coefficients C_D are approximately used by assuming from analogous example in steady flow theory following after Camfield[7]. The results are not necessarily good on the whole range, however the mechanism generating dynamic wave force on the wall seems to be roughly explained. Values calculated from mean experimental velocities would be obtained as an envelope of these groups of lines, if many measuring points are set.

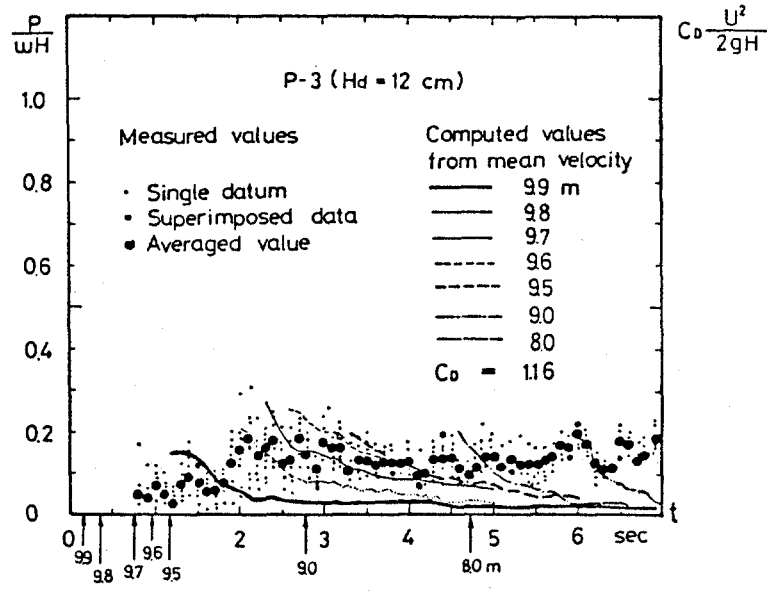

Fig.13 Comparison of computed drag forces with experimental dynamic wave forces in the case of P-3

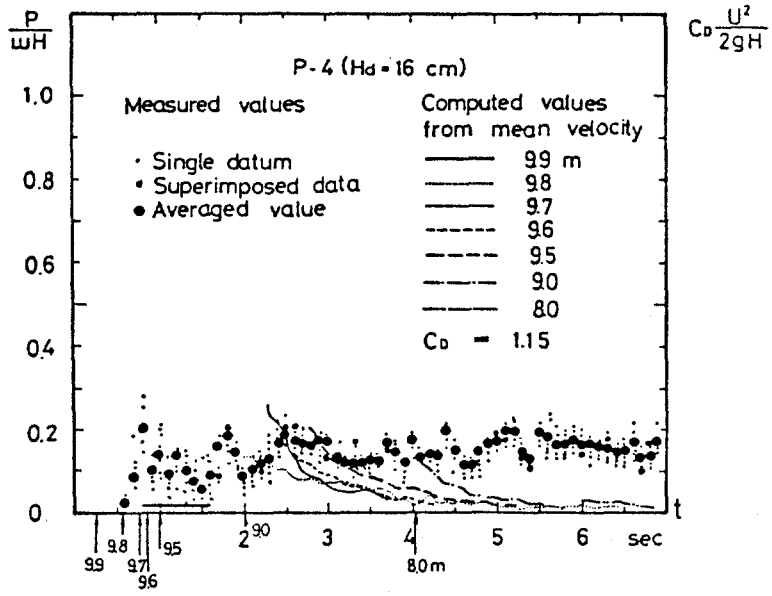

Fig.14 Comparison of computed drag forces with experimental dynamic wave forces in the case of P-4

Further, inertia force is generated by incident surge just after colliding of the surge front portion, however it is not so large and rather less than drag force by the reflected bore as a whole, so it is here disregarded.

In the result, dynamic wave force on the wall was found to be generated mainly by drag force and the magnitude of dynamic wave force of tsunami bore measured in the case was round 10~40 % of hydrostatic wave force.

IV. CONCLUSION

If steady flow theory by the author for analysis of tsunami when overflowing a wall is applied to wave height and velocity of both reflected bore in front of the vertical wall and transmitted surge to rear of it, the values near peak were seen to be roughly explained by the theory, though there is a little time lag affected by rising surge front portion.

Drag force was computed from the mean velocity in the section of reflected bore in front of the vertical wall and was compared with measured dynamic wave force on the wall. Consequently, the dynamic wave force on the wall was found to be generated mainly by the drag force. And the magnitude of the dynamic wave force in the case was round 10~40 % of the hydrostatic force obtained from water level at the wall site.

Therefore, if wave height and velocity of an incident tsunami surge near at the site of tsunami protection wall are given by numerical computation in the case without wall, the wave height and velocity near the peak of both reflected bore in front of the wall and transmitted wave in rear of it are approximately computed by the steady flow theory in the case with wall, and the maximum wave force is computed at the same time as well, so it is possible to design the tsunami protection wall and to estimate its construction effect.

ACKNOWLEDGEMENTS

The author expresses his gratitude to Mr. Katsushi Koga at Co.Ltd., Tokyo Kyuei, who was graduated from the postgraduate cource of Engineering Department, Nagasaki University, Mr. Ken-ichi Murohara at Arai-gumi Co. Ltd., who was graduated from the Department of Civil Engineering, Nagasaki University and Technical Official Yasushi Hirayama at the Faculty of Engineering, Nagasaki University, for their colaborative work to complete the present paper.

REFERENCES

1) Cumberbatch, E. : The Impact of a Water Wedge on a wall ; Journal of Fluid Mechanics, Vol. 7, 1960, pp. 353~373.
2) Fukui, Y., Nakamura, M., Shiraishi, H. and Y. Sasaki : Hydraulic Study on Tsunami ; Coastal Engineering in Japan, Vol. 6, 1963, pp. 67~82.
3) Cross, R. H. : Tsunami Surge Forces ; Proc. of ASCE, Vol. 93, No. WW4, Nov. 1967, pp. 201~231.
4) Nakamura, S. : Study on Transformation and Control of Long Wave ; A Doctorate Dissertation, Kyoto University, Aug. 1974, pp. 153~165 (in Japanese).
5) Togashi, H., Yamaguchi, S. and Y. Hirayama : On The Effect of Tsunami Protection Gate and its Design Wave Pressure ; Proc. of the 20th Japanese Conf. on Coastal Eng., JSCE, Nov. 1973, pp. 151~155 (in Japanese).
6) Iwasaki, T. and H. Togashi : On the Overland Flow of Tsunami and Effectiveness of Wall as a Counter Measure ; Coastal Engineering in Japan, Vol. 11, Dec. 1968, pp. 69~83.
7) Camfield, F. E. : Tsunami Engineering ; U.S. Army, Corps of Engineers, Coastal Engineering Research Center, Special Report No. 6, Feb. 1980, pp. 177~183.

EXTREME VALUES OF TSUNAMI MAGNITUDES

Junji KOYAMA*, Masahiro Kosuga#, and Ziro SUZUKI*

*Geophysical Institute, Faculty of Science
Tohoku University, Sendai 980 JAPAN

#Department of Earth Sciences, Faculty of Science
Hirosaki University, Hirosaki 036 JAPAN

ABSTRACT

Global earthquake-magnitude data in the period 1897 to 1980 are subject to a statistical analysis of extreme values in order to study the largest magnitude of future earthquakes. Since the actual frequency-magnitude data are not uniform in any way, we look for a method which would not be dependent on the assumptions of minimum magnitude values in the data-sets and of probability distribution functions. Although the maximum magnitude value is considered to be due to the saturation of the magnitude scale, it is shown that the value is related to the largest size of earthquake sources. Estimated maximum magnitude is converted into the maximum possible tsunami magnitude from a relation of

$$m = 3.9\, M_s - 28.6.$$

Results show that in most of the regions the maximum tsunami magnitudes calculated are compatible to and/or a little larger than those ever recorded, while in some regions the largest earthquakes ever registered have excited larger tsunami than calculated. This suggests that the largest tsunami magnitude in each seismic region ever registered is a good measure for the tsunami hazard reduction programs. Discussion is further extended to investigate the physical basis of some empirical relations concerning on tsunami magnitude and earthquake source parameters.

INTRODUCTION

Attempts have been made to estimate the maximum value of earthquake magnitudes from catalogue data (e.g., Howell, 1981; Kijko, 1984; Utsu, 1974; Yegulalp & Kuo, 1974). Although they have extended the mathematical application of extreme-value statistics to seismology, the actual data are no longer uniform nor complete so as to satisfy the mathematical requirements. Some are biased in small magnitudes because of the limitted dynamic range of the seismic observations and some are defective because of small number of large and great earthquakes resulting from the short observation periods. These biases and limitations of the actual data are not inherent in the physical nature of earthquake sources but in the artificial defects of the earthquake catalogues.

All the above analyses considered the functional forms of probability and tested the goodness of fit with regard to summed numbers of frequency-magnitude histograms. The summation considerably smooths the actual data so that in some cases the functional forms are totally under the controll of small number of the data at lower and upper magnitude-values which are due to the artificial defects mentioned above.

Recent trend in seismology is to quantify the earthquake sources in terms of physical parameters such as seismic moment, fault length and width (e.g., Kanamori & Anderson, 1975; Purcaru & Berckhemer, 1982). Although the earthquake magnitude is a kind of empirical ruler but not a physical scale, its physical background has been investigated on the basis of modern quantitative seismology (Kanamori & Anderson, 1975; Koyama & Shimada, 1985). Furthermore, surface-wave magnitude M_S of major earthquakes in the world for the period from 1897 to 1980 has been re-evaluated by Abe (1981, 1984) and Abe & Noguchi (1983). M_S scale thus revised is considered to be more uniform than those ever introduced.

We have made a catalogue from the above studies by Abe and Noguchi which consists of 1130 major earthquakes. We study M_S values of this catalogue in seismic region-by-region to estimate the largest possible earthquake in each seismic region. The goal of this paper is not to introduce a probability function to fit the data but to investigate the extreme strength of tsunami from earthquake magnitudes in worldwide seismic regions.

MAXIMUM MAGNITUDE FROM STATISTICS OF EXTREMES

Figure 1 shows a frequency-magnitude distribution for 99 major earthquakes in and near Japan. It will be found that the data are truncated for $M_S < 7.0$, which is due to non-uniformity of the catalogue for earthquakes smaller than 7.0. In spite of the circumstances, the distribution pattern in Fig. 1 would be approximately described by a Rayleigh distribution of

probability density in terms of the random variable of magnitude x as

$$P_R(x) = 2(x-M_{in})/s^2 \exp\{-(x-M_{in})^2/s^2\} \qquad x \geq M_{in} \qquad (1)$$

where M_{in} is a minimum magnitude in the catalogue. Mode (the most probable value), M_{ax} of large earthquake-magnitude values is expressed from the above probability density function as

$$M_{ax} = M_{in} + s\,F(N) \qquad (2)$$

where F is a function of sampling number N of large earthquakes (Longuet-Higgins, 1952) as

$$F(N) = (\ln N)^{1/2}. \qquad (3)$$

The example in Fig. 1 gives M_{ax} = 8.26 when M_{in} is taken as 6.6, M_{ax} is 8.35 when M_{in} is assumed to be 6.5. And M_{ax} is obtained as 8.44 when M_{in} is 6.4. The difference in M_{ax}'s arising from the choice of minimum magnitudes is mostly less than 0.1 and never exceeds 0.2. Although there remains an arbitrariness in determining M_{in}, we take M_{in} by which the peak of probability density matches that of actual frequency-magnitude data. M_{in} is so determined as 6.5 for the example in Fig. 1.

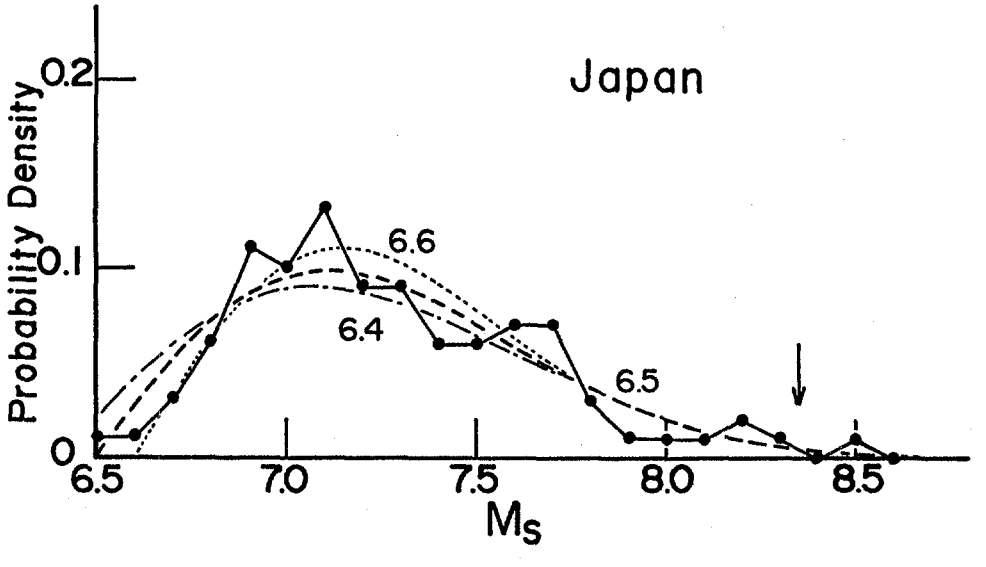

Figure 1: Magnitude-frequency plot for the major earthquakes in and near Japan. Solid circles indicate the frequency of earthquakes at each surface wave magnitude M_s normalized by the total event number. Probability density of Rayleigh distribution is calculated assuming the minimum value of magnitudes as 6.4, 6.5 and 6.6. They are illustrated by changing the curve drawings. Arrow indicates the modal extreme value of magnitudes estimated from the 6.5-dashed curve which fits the peak probability to the data peak.

If we exclude non-uniform data in the analysis, the frequency-magnitude distribution in Fig. 2 would be represented as a first approximation by an exponential distribution of probability density

$$P_E(x) = 1/b \exp\{ -(x - M_{in}) / b \} \qquad x \geq M_{in}. \tag{4}$$

We obtain the mode of large magnitude values in this case

$$M_{ax} = M_{in} + b\, G(N) \tag{5}$$

where Gumbel (1958) gave

$$G(N) = \ln N. \tag{6}$$

The example of 77 major earthquakes in and near Japan in Fig. 2 gives M_{ax} of 8.63 when M_{in} is taken as 7.0.

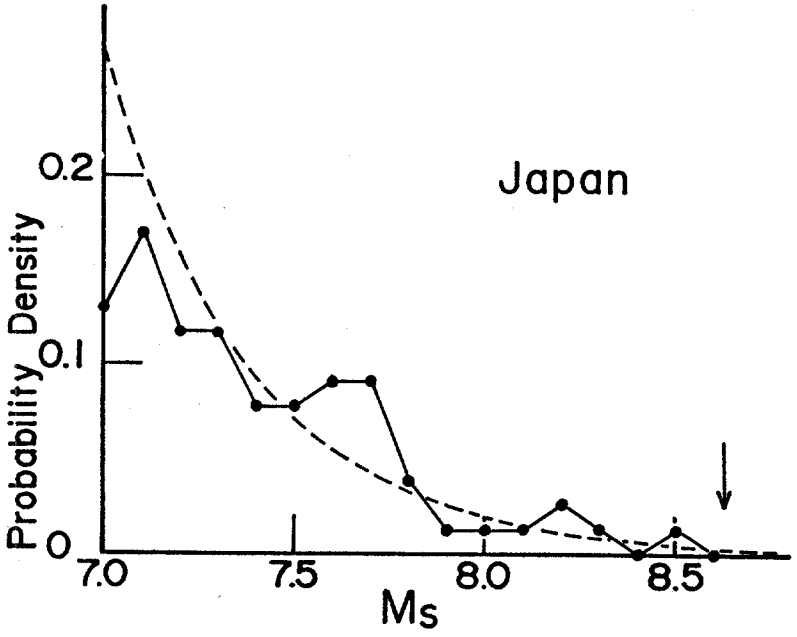

Figure 2 : Magnitude-frequency plot for the major earthquakes in and near Japan. The minimum magnitude is assumed to be 7.0 and the probability density of exponential distribution is applied to the data. Arrow indicates the modal extreme value of magnitudes.

M_{ax}'s from the exponential distribution are usually larger than those from the Rayleigh distribution. However, the difference between the two modal values in each seismic region is seldom more than 0.3. Kijko (1984) showed significant differences in estimated largest magnitude values resulting from the assumption on different probability functions. The differences are unreasonably large as much as 9.2 (Kijko, 1984). The consistent results obtained in this study is partly because we study the probability density but not the probability itself, the former of which

would not be peculiarly sensitive to the largest earthquake ever recorded.

MAXIMUM MAGNITUDE IN WORLDWIDE SEISMIC REGIONS

Most of major earthquakes in the world occur along the circum-Pacific area. Eight seismic regions are introduced considering the tectonics and seismicity. Table 1 lists the region names and west bottom- and east top-coordinates of each region within which earthquakes being located are analyzed. Some regions are taken to be overlapped with adjacent regions.

Table 1 : Seismic Regions.

Region Name	Left Bottom-	Right Top-Coordinates
Aleutian-Alaska	45.0 N 164.0 E	65.0 N 145.0 W
Kurile-Kamchatka	44.0 N 146.0 E	54.0 N 164.0 E
Japan	23.0 N 122.5 E	44.0 N 147.0 E
Philippine Sea	5.0 N 115.0 E	36.0 N 150.0 E
New Guinea-Fiji	23.3 S 135.0 E	5.0 N 180.0 E
Tonga-Kermadec	40.0 S 180.0 W	10.0 S 160.0 W
South America	60.0 S 85.0 W	5.0 N 68.0 W
Central America	8.0 N 110.0 W	23.3 N 80.0 W

Magnitude of largest possible earthquakes is calculated as discussed previously in each seismic region. Frequency-magnitude distribution in each seismic region is shown in Fig. 3 for Rayleigh distribution and in Fig. 4 for exponential distribution. Rayleigh and exponential estimates and their average are summarized in Table 2. Table 3 lists the largest earthquake ever registered in each seismic region in addition to the estimated maximum magnitude.

Some earthquakes which occurred in lands are also included in the analysis, although they did not excite any tsunami. This is because we aim to estimate the potential strength of tsunami excitation by seismic region by region through the maximum magnitude of earthquakes and because the number of inland earthquakes is very small. The earthquake catalogue deals with the seismicity of the world for about 100 years, however, the period may not be long enough to discuss the whole history of some subduction zone tectonics.

Roughly speaking, the number of earthquakes would increase linearly as a function of the period, if the seismicity is more or less stationary. The maximum earthquake magnitude for two-hundred-year seismicity would be obtained by doubling the event number in Table 2. From such the hypothetical data we always observe larger maximum-magnitude values than those in Table 2. However the difference between the present and hypothetical estimates is mostly as small as 0.1. Because the difference

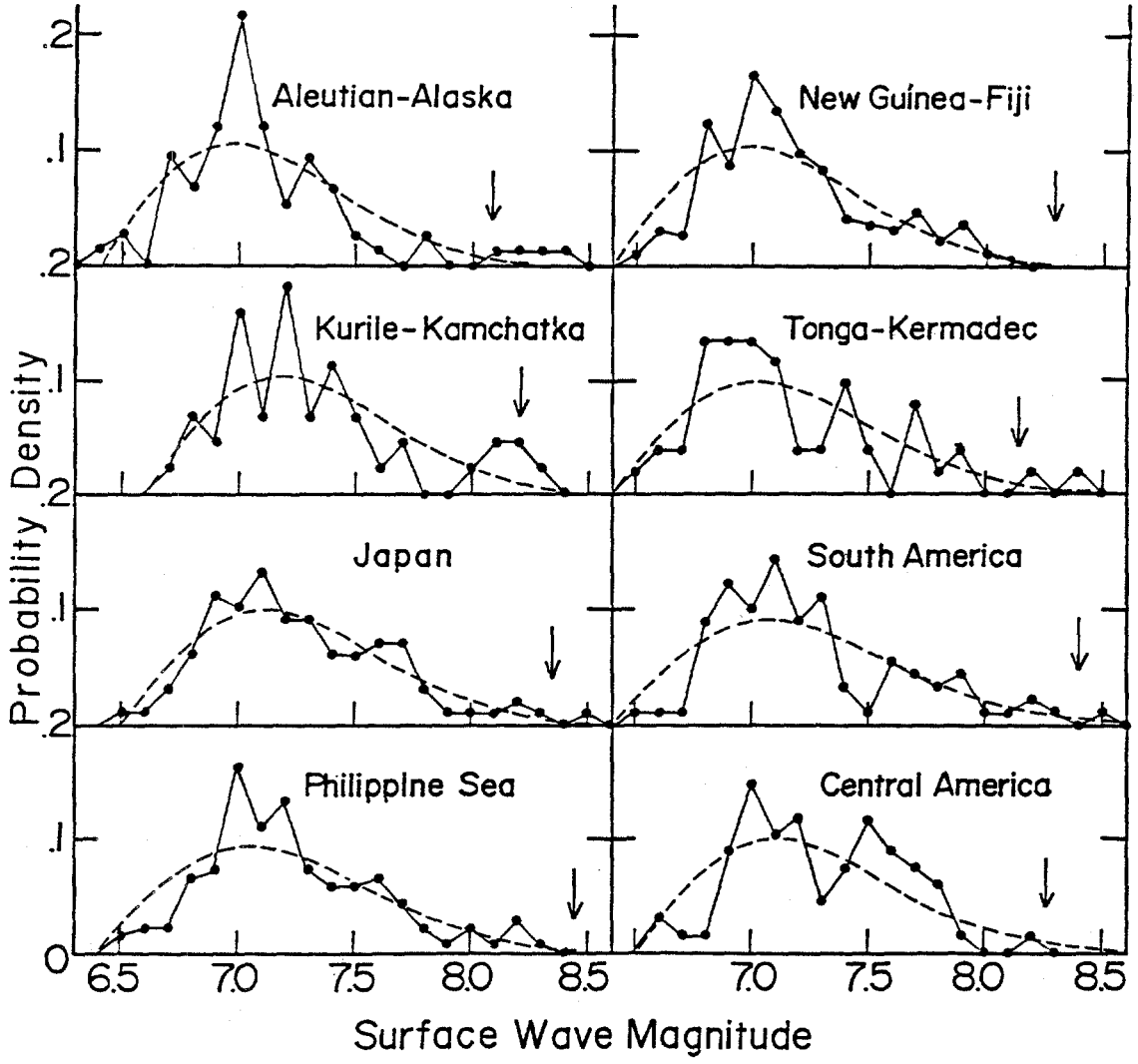

Figure 3: Magnitude-frequency plot in the worldwide seismic regions. Rayleigh probability distribution is assumed to fit the data. Symbols are the same as those in Fig. 1.

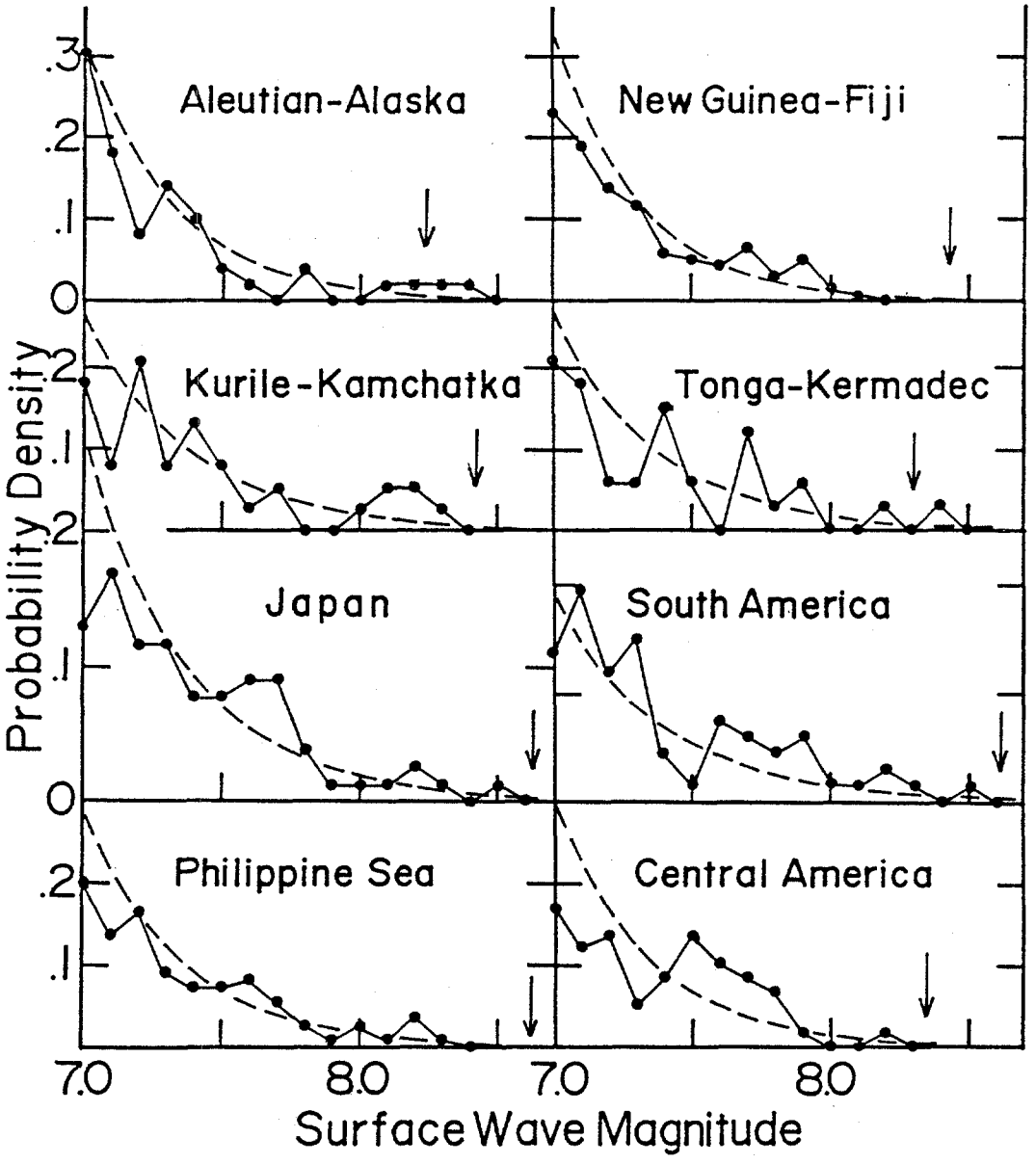

Figure 4: Magnitude-frequency plot in the worldwide seismic regions. The data are excluded in the analysis of which magnitudes are smaller than 7.0. Symbols are the same as those in Fig. 2.

never exceeds more than 0.2, we consider that the error arising from the limitation of the data period is not so significant in the present study.

It will be found that 1964 Alaska and 1917 Samoa Islands earthquakes are the exceptionally large events beyond the statistical estimations. Except for above two regions, Aleutian-Alaska and Tonga-Kermadec, the maximum magnitude of largest possible earthquakes is equal and/or somewhat larger than those ever registered.

Table 2 : Maximum magnitude in each seismic region.

Region Name	Rayleigh	No*	Exponential	No*	Average
Aleutian-Alaska	8.08	74	8.24	50	8.2
Kurile-Kamchatka	8.21	44	8.42	38	8.3
Japan	8.35	99	8.63	77	8.5
Philippine Sea	8.44	136	8.62	109	8.5
New Guinea-Fiji	8.29	193	8.43	137	8.4
Tonga-Kermadec	8.14	52	8.30	33	8.2
South America	8.40	90	8.61	66	8.5
Central America	8.26	68	8.35	58	8.3

No^* is the number of earthquakes in the analysis.

SIGNIFICANCE OF THE MAXIMUM MAGNITUDE

Often discussed in the literatures is the saturation of magnitude scales for large and great earthquakes. Aki (1972) and Kanamori & Anderson (1975) showed a relation between earthquake magnitudes and amplitudes of narrow-band earthquake source spectra. They have derived a relation between surface-wave magnitude M_s and seismic moment M_o for large and great earthquakes as

$$\log M_o \propto 3 M_s. \qquad (7)$$

Because M_o is a parameter representing the total work done by an earthquake, the above equation suggests that no matter how the earthquake energy becomes large, M_s would not increase so drastically as M_o. It increases in proportion to a logarithm of one third power of the total energy.

Recently, Koyama & Shimada (1985) studied surface-wave magnitude and fault area S for large earthquakes in the world and they showed that M_s for great earthquake is a measure of the logarithm of square root of earthquake source sizes: The total energy radiated is a function of both the amount of displacement at each source point and the dimension of source area. This is parameterized by M_o. On the other hand, the peak

amplitude of seismic waves for M_s determination is a function of instantaneous energy flux.

Surface-wave magnitude M_s, as its definition states, is determined by an ordinary logarithm of peak surface-wave amplitude with a period of about 20 sec. The wavelength of such seismic waves is approximately 70 to 80 km. It corresponds to the size of an earthquake with M_s = 7.5 (Aki, 1972). Earthquakes with M_s = 8 and over have source dimensions of more than hundreds of km's which are by far larger than the wavelength for M_s determination. Therefore, we can reasonably consider that the wavelength of 20 sec surface-waves is very short in comparison with the source dimensions of large and great earthquakes.

Table 3 : Maximum Magnitudes Estimated and Registered.

Seismic Region	Earthquake Magnitude		Tsunami Magnitude	
	Estimated	Registered	Estimated	Registered
Aleutian-Alaska	8.2	8.4 (1964)	3.2	4 (1964) A
Kurile-Kamchatka	8.3	8.3 (1952)	3.8	4 (1952) A
Japan	8.5	8.5 (1933)	4.5	4 (1896) B
Philippine Sea	8.5	8.3 (1923)	4.6	3.6(1923) B
New Guinea-Fiji	8.4	8.1 (1934)	4.0	
Tonga-Kermadec	8.2	8.4 (1917)	3.4	3 (1917) B
South America	8.5	8.5 (1960)	4.5	4.5(1960) A
Central America	8.3	8.2 (1932)	3.8	2 (1932) B

Last column indicates references A: Cox & Carayannis(1976), and B: Carayannis(1977).

The excitation of short waves is briefly expressed following Koyama & Shimada (1985): Let us consider a heterogeneous fault with a total areal size S. Narrow frequency-band seismic energy radiated from the random fracture of fault heterogeneities (fault patches) will be

$$E \simeq k \overline{e^2} K \qquad (8)$$

where k is a number of fracturing fault patches in a unit time, $\overline{e^2}$ is an average narrow-band energy radiated from a fault patch and K is the total number of fault patches on the fault. If a number density p of fault patches in a unit fault area is considered, we have

$$K = p S. \qquad (9)$$

We approximate the amount of seismic wave energy as a square mean amplitude multiplied by its wave duration. Parseval's theorem gives an

approximate expression of a square mean value $\overline{a^2}$ of seismic waves as

$$\overline{a^2} \propto c_1 E / (S^{1/2}/v_R) \qquad (10)$$

where the denominator of the right-hand side represents a duration of short-period seismic waves observed on seismograms (Koyama & Zheng, 1985), and c_1 is a constant. In other words, the duration is assumed to be a time constant of a rupture propagation on the fault with a rupture velocity v_R. Setting $M_{in} = 0$ in (2) and (5), the maximum amplitude of narrow-band seismic waves is

$$a_{max} = (\overline{a^2})^{1/2} F(K) \qquad (11)$$

where (3) or (6) will be used for above F. More explicitly, if p and $\overline{e^2}$ would not change large by seismic region by region, we have

$$a_{max} \propto c_2 S^{1/2} F(K) \qquad (12)$$

where c_2 is a constatnt , and k is approximated similarly to (10) as

$$k \simeq K / (S^{1/2} / v_R). \qquad (13)$$

Surface-wave magnitude of large and great earthquakes will be considered on a basis of the short-wave approximation as an ordinary logarithm of (12) (Koyama and Shimada, 1985). Logarithm of the function F in (12) varys insignificantly for large values of K (say, for K > 50). Therefore, it is expected that M_s is proportional to 0.5 log S from the above discussion. This has been demonstrated by Koyama & Zheng (1985) for large and great earthquakes in the world as

$$\log S \simeq 2 M_s - 1.5 \qquad (14)$$

where S is in the unit of cm^2.

Even though it seems that there is a saturation of the magnitude scale, the magnitude is shown to be closely related to square root of the fault area. This is another interpretation of the maximum magnitude independent of that in (7). The maximum magnitude obtained in the previous section, consequently, will be considered as some kind of upper-bound size effects of earthquake sources in various seismic regions.

RETRIEVAL OF TSUNAMI MAGNITUDE

It has been empirically studied the relations between tsunami energy and earthquake magnitude. However, the tsunami energy should be a measure of the total deformation of the ocean bottom due to large earthquakes. Hatori (1979) studied a relation between seismic moment and tsunami

magnitude m of tsunamigenic earthquakes;

$$\log M_o = 0.77\ m + 26.89. \qquad (15)$$

where M_o is in the unit of dyne.cm. This means, in turn, that tsunami magnitude can be estimated immediately when seismic moment of an earthquake is evaluated.

Abe (1975) derived a simple relation between M_o and S as

$$M_o = 1.23 \times 10^{7}\ S^{3/2} \qquad (16)$$

which has been reconfirmed by Kajiura (1981) for interplate earthquakes. Then the inverse of (15) (Takemura & Koyama, 1983),

$$m = 1.3 \log M_o - 34.9 \qquad (17)$$

is applicable to combine the maximum magnitude to the estimate of ultimate strength of tsunami. From (14), (16) and (17), we have an approximate relation

$$m = 3.9\ M_s - 28.6. \qquad (18)$$

This equation gives an estimate of the tsunami strength from the earthquake magnitude. Although the period of seismic surface-waves for the earthquake magnitude-determination is very short compared to the tsunami period, the wavelengths are more or less the same order each other. So that, we would not be talking about two completely different parameters in mixed up. Before applying (18) to the estimation of ultimate tsunami strength from the earthquake magnitude, let us check the equation from the data. Fig. 5 shows tsunami magnitude and surface wave magnitude for the earthquakes near Japan and major earthquakes in the world. The equation is a fairly good approximation indicating the upper bound of tsunami magnitude for a given earthquake magnitude except for some data of tsunami earthquakes (low-frequency earthquakes which do not radiate seismic waves effectively) and for those of minimum tsunami-magnitude earthquakes.

Table 3 summarizes the maximum tsunami magnitude thus calculated from (18) and also the largest tsunami ever registered in each seismic region. We notice that the 1964 Alaska earthquake generated the tsunami unexpectedly larger than the estimate. The maximum tsunami magnitude estimated in the Philippine sea is very large, because the seismicity includes the catastrophic large earthquakes near Japan like as 1923 Kwanto, 1944 Tonankaido, and 1946 Nankaido earthquakes. The difference between estimated and registered tsunami magnitudes is considerably large in Central America. This may be partly because the recurrence time-interval of large earthquakes in Central America is short, about 34.5 years (Rikitake, 1976), compared to the period of the catalogue. Or there

might be some difference in the tsunami excitation mechanisms for Central American earthquakes. In other seismic regions the maximum strength of tsunamis would be more or less the same order of magnitudes ever registered.

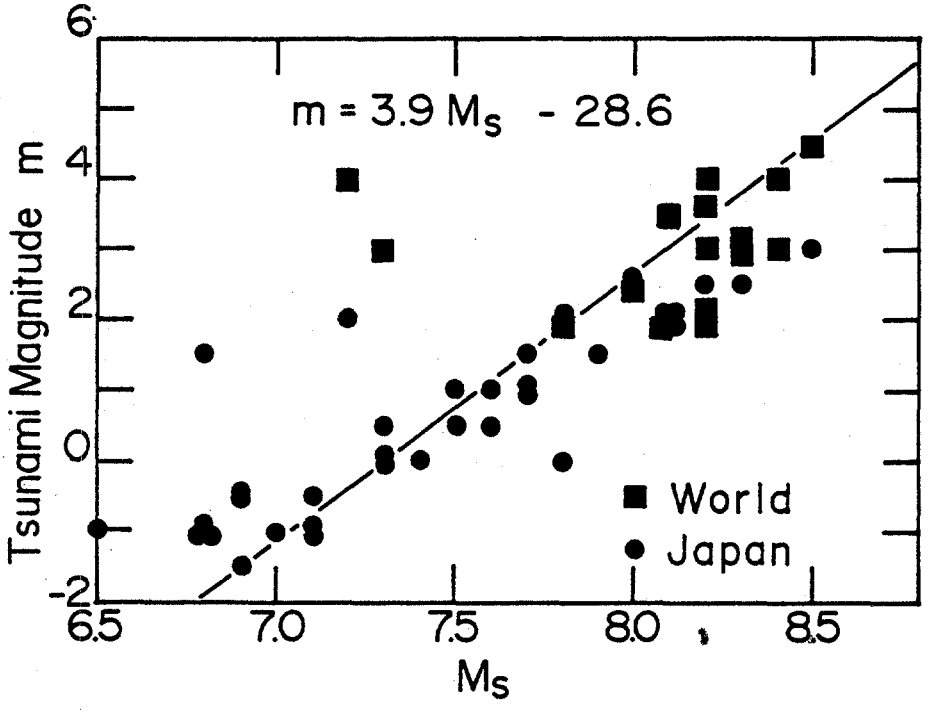

Figure 5 : Tsunami magnitude and surface wave magnitude for earthquakes near Japan (circles) and great earthquakes in the world (squares). The data are mainly quoted from Abe (1979; 1981b), Hatori (1971; 1979) and Iida (1984). Equation in the figure would be valid for earthquakes larger than 7.5.

PHYSICAL BASIS OF TSUNAMI MAGNITUDE

Empirical relations between tsunami magnitude and earthquake source parameters have been derived as (15), (17) and (18). They are applied to estimate the possible largest tsunami-magnitude from seismological data. Here, we study the physical meanings of the relations more in detail.

The definition of tsunami magnitude states (Kajiura, 1981),

$$m = \log_2 H_{max} \qquad (19)$$

where H'_{max} is the maximum tsunami height on tide-gage records and/or maximum inundation height (Hatori, 1979). The definition is essentially the same even when we take into account the effects of geometrical diminution due to tsunami propagation and of magnification due to

difference in bathymetric depths at the source and receiver(Hatori, 1979).

Tsunamis excited by submarine earthquakes are usually studied under the long-wave approximation, because the wavelength of tsunamis is almost always very large compared to the bathymetric depths (Kajiura, 1981; Takahasi, 1942). The maximum tsunami height is, in case of the long-wave approximation, strictly related to the maximum vertical deformation, D_{max}, of the ocean bottom (Ben-Menahem & Rosenman, 1972). Therefore, we have slightly changing (19) as

$$m \propto \log_2 D_{max} \qquad (20)$$

Combining (14), (18) and (20), we obtain a relation of

$$\log D_{max} \propto 0.59 \log S \qquad (21)$$

The above relation shows that the maximum value of the ocean bottom vertical deformation is proportional approximately to the square root of the fault area.

This is similar to the relation between the dislocation on fault planes and the size of fault areas. The long-period seismology has shown its physical basis from the assumption of similarity law among the fault parameters (Aki, 1972; Kanamori & Anderson, 1975). Furthermore, the similarity law among fault length L, width W and dislocation D would give

$$M_o = \mu DLW \propto c_3 D_{max}^3 \qquad (22)$$

where μ is the rigidity in the source region, and c_3 is a constant independent of the earthquake source size. Inserting (22) into (20), we obtain

$$m \propto \log_2 D_{max} \propto 1.11 \log M_o \qquad (23)$$

The above equation is quite similar to the empirical relation (17) by Hatori (1979). Therefore, we could conclude that the empirical relations concerning on the tsunami magnitude are manifesting the similarity law among earthquake source parameters predicted by the long-period seismology.

CONCLUSIONS

We studied the statistics of extreme values to estimate the maximum magnitude of future earthquakes. The maximum magnitude is shown to be related to the maximum size of earthquake faults and not attributed to the saturation of magnitude scale. The earthquake catalogue analyzed in the present study is composed of the seismicity in the world for about one

hundred years. Of course, the period would not be sufficiently long enough to know the whole history of the tectonics in each seismic region. However, the maximum tsunami magnitude from the analysis predicts the ultimate strength of tsunamis which is almost identical to and/or a little larger than those ever registered in each seismic region. Therefore, the maximum strength of future tsunamis will be set, for the tsunami hazard reduction programs, to the maximum tsunami magnitude ever registered in the documents as far as the seismological results are concerned.

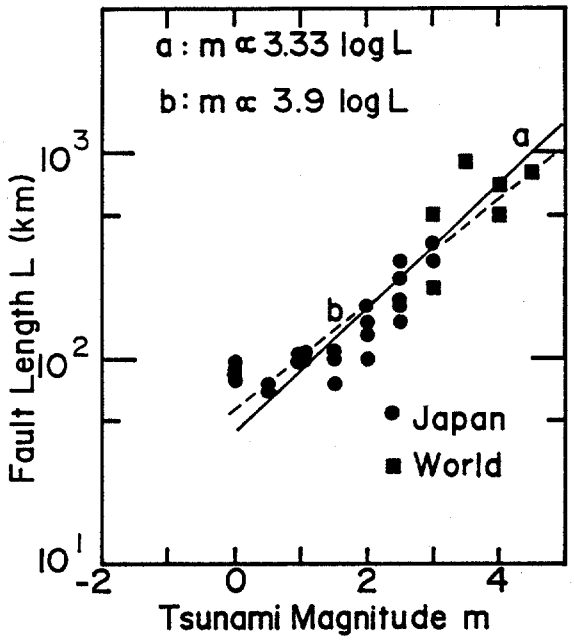

Figure 6 : Tsunami magnitude and fault length for earthquakes near Japan and great earthquakes in the world. Relation a: m ∞ 3.33 log L is from (22) and (23) by solid line. Relation b: m ∞ 3.9 log L is from (17) and (22) by broken line in the figure.

Empirical relations between tsunami magnitude and earthquake source parameters are studied in a physical manner. And they are understood as a first approximation by the similarity law among the earthquake source parameters which is common in the long-period seismology (Aki, 1972; Kanamori & Anderson, 1975). If we only assume the similarity law instead of the empirical relations such as (15) and (17), an equation is obtained from (14), (16) and (23) as

$$m \simeq 3.33\, M_s - 23.8 \qquad (24)$$

in place of (18). It looks that (24) is a better representation for the data in Fig. 5 than (18). However, we do not think the difference in (18) and (24) is significant, because the scatter of the data is extremely large. The essential point is that the similarity law among the faulting parameters from long-period earthquake-source studies explains the

empirical relations on the tsunami magnitude. Fig. 6 summarizes fault length of earthquakes near Japan and major earthquakes in the world in terms of tsunami magnitude of corresponding earthquakes. The similarity law for (22) and (23) would predict a relation between tsunami magnitude and fault length shown by a solid line a in the figure. The empirical relation (17) suggests a relation b by broken line in the figure. Because fault lengths are independently determined and are better constrained source parameters than estimated source areas (Lay et at., 1982), our understanding on the tsunami excitation from the similarity law of faulting parameters is reconfirmed.

Izutani & Hirasawa (1985) investigated the duration of strong ground motions in short distances to estimate the fault length in order to improve the tsunami warning system in Japan. Takemura & Koyama (1983) applied the instantaneous seismic moment determination from forecoming seismic waves to evaluate the tsunami strength more precisely. (20) does suggest the importance of the maximum deformation of the ocean bottom or the maximum amount of dislocation on the fault for the tsunami excitation as well as fault strength (length and width) and net strength (seismic moment).

Acknowledgement

This study is partly supported by the Tojiro Ishihara Scholarship, Association for Disaster Prevention Researches, Kyoto, Japan and also by the Grant Aid for Scientific Research, the Ministry of Education, Japan.

References

Abe, K., 1975, Reliable estimation of the seismic moment of large earthquakes, J. Phys. Earth, 23, 381-390.

Abe, K., 1979, Size of great earthquakes of 1837-1974 inferred from tsunami data, J. Geophys. Res., 84, 1561-1568.

Abe, K., 1981, Magnitudes of large shallow earthquakes from 1904 to 1980, Phys. Earth Planet. Inter., 27, 72-92.

Abe, K., 1981 b, Physical size of tsunamigenic earthquakes of the northwestern Pacific, Phys. Earth Planet. Inter., 27, 194-205.

Abe, K., 1984, Complements to "Magnitudes of large shallow earthquakes from 1904 to 1980", Phys. Earth Planet. Inter., 34, 17-23.

Abe, K. and S. Noguchi, 1983, Revision of magnitudes of large shallow earthquakes, 1897-1912, Phys. Earth Planet. Inter., 33, 1-11.

Aki, K., 1972, Scaling law of earthquake source time-function, Geophys. J. Roy. Astron. Soc., 31, 3-25.

Ben-Menahem, A. and M. Rosenman, 1972, Amplitude patterns of tsunami waves from submarine earthquakes, J. Geophys. Res., 77, 3097-3128.

Carayannis, G. P., 1977, Catalog of tsunamis in Hawaii, World Data Center A, Rep. SE-4, 1-78.

Cox, D. C. and G. P. Carayannis, 1976, Catalog of tsunamis in Alaska, World Data Center A, Rep. SE-1, 1-43.

Gumbel, E.J., 1958. Statistics of extremes, Columbia Univ. Press, New York, pp. 75-254.

Hatori, T., 1971, Tsunami sources in Hokkaido and southern Kuril regions, Bull. Earthq. Res. Inst., Tokyo Univ., 49, 63-75.

Hatori, T., 1979, Relation between tsunami magnitude and wave energy, Bull. Earthq. Res. Inst., Tokyo Univ., 54, 531-541.

Howell, B.F., Jr., 1981, On the saturation of earthquake magnitudes, Bull. Seism. Soc. Am., 71, 1401-1422.

Iida, K., 1984, Catalog of tsunamis in Japan and its neighboring countries, Special Report, Aichi Inst. Tech., 1-52.

Izutani, Y. and T. Hirasawa, 1985, Rapid estimation of fault parameters for tsunami warning, submitted to Proc. Intern. Tsunami Symp. '85.

Kajiura, K., 1981, Tsunami energy in relation to parameters of the earthquake fault model, Bull. Earthq. Res. Inst., Tokyo Univ., 56, 415-440.

Kanamori, H. and D.L. Anderson, 1975, Theoretical basis of some empirical relations in seismology, Bull. Seism. Soc. Am., 65, 1073-1095.

Kijko, A., 1984, Is it necessary to construct empirical distributions of maximum earthquakes magnitudes? Bull. Seism. Soc. Am., 74, 339-347.

Koyama, J. and N. Shimada, 1985, Physical basis of earthquake magnitudes: An extreme value of seismic amplitudes from incoherent fracture of random fault patches, Phys. Earth Planet. Inter., 40, 301-308.

Koyama, J. and S.-H. Zheng, 1985, Excitation of short-period body-waves by great earthquakes, Phys. Earth Planet. Inter., 37, 108-123.

Lay, T., L. Ruff and H. Kanamori, 1982, The asperity model and the nature of large subduction zone earthquakes, Earthq. Predict. Res., 1, 3-71.

Longuet-Higgins, M.S., 1952, On the statistical distribution of the heights of sea waves, J. Mar. Res., 11, 245-266.

Purcaru, G. and H. Berckhemer, 1982, Quantitative relations of seismic source parameters and a classification of earthquakes, Tectonophysics, 84, 57-128.

Rikitake, T., 1976, Recurrence of great earthquakes at subduction zones, Tectonophysics, 35, 335-362.

Takemura, M. and J. Koyama, 1983, Seismic source spectrum of tsunami and ordinary earthquakes: A quantitative estimation of tsunami from forecoming seismic wave, Tohoku Geophys. J., 29, 115-128.

Utsu, T., 1974, A three-parameter formula for magnitude distribution of earthquakes, J. Phys. Earth, 22, 71-85.

Yegulalp, T.M. and J.T. Kuo, 1974, Statistical prediction of the occurrence of maximum magnitude earthquakes, Bull. Seism. Soc. Am., 64, 393-414.

THE INFLUENCE OF THE EARTH'S ROTATION ON THE ENERGY CHARACTERISTICS OF TSUNAMI WAVES

S. S. Voit, and B. I. Sebekin
Wave Dynamic Laboratory Institute of Oceanology of the USSR Academy of Science, 23 Krasikova, Moscow, USSR-117218

ABSTRACT

The influence of the Coriolis force on the propagation of tsunami waves in the offshore ocean and on the interaction of tsunami waves with underwater slopes and continental shelves are examined. The rotation of the earth can strongly effect the tsunami characteristics near the region of formation of tsunamis. The rotation provides motions of different spatial and time scales. Together with relatively short-periodic gravitational waves the slow curl motions occur. During this process some part of the energy, which is transmitted to the ocean with the seismic bottom mot ions, accumulates in the region of the disturbance. This leads to a reduction of the barotropic wave energy and tsunami amplitude. The direction of the tsunami radiation varies and the energy flow transfered by the waves is redistributed.

Let us qualitatively evaluate the role of the Earth's revolution in the processes of propagation of tsunami waves. The seismic source inducing the tsunami lasts for a period, which is small in comparison with the characteristic wave's period. Assuming that the moving of the bottom is infinitely short, we inquire what is the most simple scheme of tsunami generation as a result of initial deflection of the free surface from the equilibrium position. This model enables us easily to calculate the initial total energy $\mathcal{E}_0$, which is transmitted to the ocean during underwater earthquakes

$$\mathcal{E}_0 = \frac{1}{2}\rho g \int_{-\infty}^{+\infty}\int \xi_0^2(x,y)\,dx\,dy$$

where ρ denotes density, g - the acceleration of gravity, ξ_0 - initial deflection of the free surface. To follow the flow resulting from the initial disturbance we shall examine the linear equations of the long wave approximation.
Let us consider the Coriolis parameter constant f.

$$\frac{\partial u}{\partial t} - fv = -g\frac{\partial \xi}{\partial x}\,,\quad \frac{\partial v}{\partial t} + fu = -g\frac{\partial \xi}{\partial y}\,,\quad \frac{\partial \xi}{\partial t} + H\left(\frac{\partial u}{\partial x} + \frac{\partial v}{\partial y}\right) = 0 \qquad (1)$$

where u, v denotes the velocity components in directions x, y, H - denotes the depth of the basin. Using methods of integral transformations one can easily obtain the solution of the system (1),

$$u(\underline{R},0) = v(\underline{R},0) = 0\,,\quad \xi(\underline{R},0) = \xi_0(R) \qquad \underline{R} = (x,y)$$

$$\xi(\underline{R},t) = \xi_g(\underline{R}) + gH\int |\underline{\kappa}|^2 A(\underline{\kappa})\, e^{i\underline{\kappa}\underline{R}}\, d\underline{\kappa}$$

$$u(\underline{R},t) = u_g(\underline{R}) + ig\int \left[\ell f A(\underline{\kappa}) - \kappa B(\underline{\kappa})\right] e^{i\underline{\kappa}\underline{R}}\, d\underline{\kappa}$$

$$v(\underline{R},t) = u_g(\underline{R}) - ig\int \left[\kappa f A(\underline{\kappa}) + \ell B(\underline{\kappa})\right] e^{i\underline{\kappa}\underline{R}}\, d\underline{\kappa}$$

$$\underline{\kappa} = (\kappa,\ell)\,,\qquad \underline{R} = (x,y) \qquad (2)$$

$$A(\underline{\kappa}) = \bar{\xi}_0(\underline{\kappa})\cdot\frac{\cos\sigma t}{\sigma^2}\,,\quad B(\underline{\kappa}) = \xi_0(\underline{\kappa})\cdot\frac{\sin\sigma t}{\sigma}$$

$$\sigma^2 = f^2 + gH|\kappa^2|\,,\qquad \xi_0 = \frac{1}{4\pi^2}\int \xi_0(\underline{R})\, e^{-i\underline{\kappa}\underline{R}}\, d\underline{R}$$

The first member in the right part of the equation (2) determines the stable geostrophic motion.

$$\xi_g(\underline{R}) = \int f^2 A(\underline{\kappa})\, e^{i\underline{\kappa}\underline{R}}\, d\underline{\kappa}$$

$$u_g = -\frac{g}{f}\frac{\partial \xi_g}{\partial y}, \qquad v_g = \frac{g}{f}\frac{\partial \xi_g}{\partial x}.$$

The total energy of the geostrophic motion is determined by the value

$$\mathcal{E}_g = \frac{1}{2}\int\left[\rho H(u_g^2 + v_g^2) + \rho g \xi_g\right] dR$$

Using Parseval formula let us express (3) in terms of the Fourier-transforms.

$$\mathcal{E}_g = 2\pi^2\int\left[\rho H(|\bar{u}_g|^2 + |v_g|^2) + \rho g|\xi_g|^2\right] d\kappa = 2\pi^2\rho g\int\frac{f^2}{\sigma^2}|\xi_g|\, d\kappa \qquad (4)$$

Analogously one can write the equation for the total initial energy

$$\mathcal{E}_0 = 2\pi^2\rho g\int|\bar{\xi}_0|^2\, d\kappa$$

Using the theorem one can express the geostrophic level of the free surface in the form convenient for the analysis

$$\xi_g(\underline{R}) = \frac{f^2}{2\pi g H}\int_{-\infty}^{+\infty}\int\xi_0(\alpha,\beta)K_0\left[\frac{f}{\sqrt{gH}}\sqrt{(x-\alpha)^2+(y-\beta)^2}\right]d\alpha\, d\beta$$

where $K_0(z)$ denotes Mac Donald function. With the help of the Mac Donald function we can obtain the result that the geostrophic level beyond the region of disturbance reduces exponentally.

In the differential form system (1) may be written:

$$\frac{1}{2}\frac{\partial}{\partial t}\left[\rho H(u^2+v^2) + g\rho\xi^2\right] = -H\,\mathrm{div}(\rho u) \qquad (5)$$

where ρ denotes density, ρ - deflection of the pressure from hydrostatic. Let us write equation (5) in the integral form for the cylindrical space with the contour L as a projection.

Integrating by time and space V, one can find

$$\mathcal{E}(t_2) - \mathcal{E}(t_1) = -H \int_{t_1}^{t_2} dt \int_L p u_n \, dL \qquad (6)$$

where $\mathcal{E}(t) = \frac{1}{2} \int [\rho H (u^2 + v^2) + \rho g \zeta^2] \, dS$ denotes the total energy of the system inside the space V in time moment t, S denotes space boundered the contour L. Equation (6) has a clear physical sense: the change of the total energy of the system inside the space V during time $t_2 - t_1$ is equal to the flow of the energy through the lateral surface.

The energy flow through the free surface and the bottom usually is zero. Equation E_q / E_0 determines the part of the initial energy, which remains in the space of disturbance and is not radiated by waves.

Assuming a to denote the characteristic linear scale of disturbance, the determining member in the integral (4) can be rewritten in the form:

$$\frac{f^2}{\sigma^2} = \frac{\varkappa^2}{\varkappa^2 + |k|^2}, \quad \varkappa = \frac{af}{c} \qquad c^2 = gH$$

The part of the energy transmitted to the geostrophic moving is determined in general by the value of the parameter C. For relatively nondeep regions of the ocean and long-and-narrow regions of underwater earthquakes the energy of geostrophic movements can achieve ten percent of the initial energy.

For the examining the energy characteristics of the wave radiation let us fix as a control co ntour, L, the circle of big radius R including the region of initial disturbance.

Thus

$$\mathcal{E}_w(t_2, t_1, R, \alpha) = H \int_{t_1}^{t_2} p(R\cos\alpha, R\sin\alpha) u_R(R\cos\alpha, R\sin\alpha) \, dt \qquad (7)$$

where R, α denotes polar coordinates of the point (x, y), u_R denotes normally orientated component of the velocity.

Determined this way the function $\mathcal{E}_w$ gives the distribution of the density of the energy flow during time interval $t_2 - t_1$ through the control surface. The total energy leaving the control space during this time can be calculated from

$$\mathcal{E}_w(R, t_2, t_1) = \int_0^{2\pi} \mathcal{E}_w R \, d\alpha$$

The distribution of the flow density of the wave energy in the approximation of the long-wave theory in the unilateral water can be calculated by the method, proposed in (4).

$$\mathcal{E}_w = 2\pi^2 \frac{\rho g}{a^2 R} \int_0^\infty \frac{r^2}{r^2 + \varkappa^2} \left| \bar{\xi}_0(r\cos\alpha,\ r\sin\alpha) \right|^2 r\, dr$$

where $\xi_0(\underline{\kappa})$ denote range of the initial deflection of the level.

The equation for the energy flow density obtained enables us to examine easily this characteristic in connection with the form of the initial disturbance and Coriolis effect.

The effectivity of the Coriolis factor can be qualitatively evaluted with the help of the parameter

$$\varkappa = af/c \quad , \qquad c^2 = \sqrt{gH}$$

For the axi-symetric source of wave disturbance, the Earth's revolving doesn't much affect the distribution of energy flow density.

It is well-known that the region of underwater earthquake is usually not axi-symetric. Most underwater earthquakes are elliptical with a ratio of length to width of ten. The long axis of the ellipse is of the order of hundreds of kilometeres.

For the quantitative analysis of the influence of the Earth revolving let us consider the case of initial disturbance in the form

$$\xi_0(\underline{R}) = A \exp\left[-\left(\frac{x^2}{a^2} + \frac{y^2}{b^2}\right)\right]$$

The spectrum of the initial disturbance can be easily determined as

$$\bar{\xi}_0(\underline{\kappa}) = \frac{ab\,A}{4\pi^2} \exp\left[-\frac{1}{4}\left(a^2k^2 + b^2l^2\right)\right]$$

Using formula (7), mentioned abo ve can get the analytic equation for the energy flow. The density of the flow of energy is

$$\mathcal{E}_w = \frac{\rho g Q^2}{8\pi^2 a^2 R} \left\{ \mu^{-1} + \frac{1}{2}\varkappa^2 \exp\left[\frac{1}{2}\varkappa^2\mu\right] \cdot \mathcal{E}i\left[-\frac{1}{2}\varkappa^2\mu\right] \right\} \quad (8)$$

where $\mathcal{E}i(z)$ denotes integral function, $\mu = \cos^2\alpha + \varepsilon^2\sin^2\alpha$, α denotes the azimuth of the examining point, Q denotes the amount of the water removed.

The first member in the brackets in the formula (8) means the distribution of the density of the energy flow in azimuth in non-revolving water. The second member J_2 determines the role of the effect of revolving in the diagram of radiation directions.
Value $\gamma = J_2/(J_1 + J_2)$ characterize the influence of the Coriolis factor at diagram of directions. The numerical calculations, made for the value of parameters $\varepsilon = 10^{-1}$, $\varkappa = 0{,}25$, which are in accordance with the mean conditions in the area of a forming tsunami, have shown that in the direction co linear to the big semiaxis of the ellipse. The revolving of the Earth effects not only the total reduction of wave energy, but also strongly redistributes the energy flow and increases the directioness of the radiation of energy, which is connected with geometry of the underwater earthquake source.

Literature

1. Voit S.S., Lebedev A.N., Sebekin B.I. The generation of tsunami wave by horizontal impols. The processes of disturbance and propagation of tsunami waves. The Institute of Oceanology of USSR Academy of Sciences, Moscow, 1982.

NEWS ITEM

NEW TSUNAMI RECORDER AT WAKE ISLAND

W.G. Van Dorn
Scripps Institution of Oceanography

As seems not too well known, the United States has, within the past twenty years, lost its entire tsunami database; all U.S. tide gages have been converted to six-minute sampling, which hopelessly aliases tsunami signals, and the handful of tsunami warning stations remaining record on curvinlinear analogue strip charts, which are impossible to digitize by standard tracing techniques. NOAA's tentative plans to telemeter early warning data to the TWS headquarters in Hawaii will not alleviate the research problem, for which a week's continuous data are needed.

A a first step in correcting this serious deficiency, a new, digital tsunami recording installation was completed at Wake Island in September, 1985, under funding by the National Science Foundation, and with logistics and maintenance support from the National Weather Service. Wake Island was selected for this installation because of its long history as a mid-ocean reference station (Van Dorn, 1984).

The new installation is comprised of an absolute pressure transducer beneath the existing tide house on the south side of Wake, connected hydraulically to the open sea by a 1 km copper tube, and electrically to a digital recording system in the tide house. The transducer is located in a sand-filled box at a depth of 2 m, and the 1 cm dia. tube runs south along the boat channel and over the reef face to a depth of 180m. A vertical standpipe rises above the surface where the tube joins the transducer, and the tube and standpipe comprise an hydraulic low-pass filter with a 30-sec. rolloff. This filter, together with that provided by deep immersion of the outer tube end, attenuates swell frequencies by about 40db, and completely eliminates the strong 3 min. seiche within the boat basin that dominates tide signals at Wake.

Frequency modulated signals from the transducer are amplified and passed to a central processor which performs several functions. It converts the signals to digital numbers every six seconds and stores them in a 1 megabit bubble memory. It averages them every 30 sec. and prints them on a solid-state strip chart recorder (for diagnostic purposes). It prints clock time on the chart and bubble memory every three hours. And lastly, after the memory is full (about ten days), it writes over the memory, so that the bubble only stores the most recent 10 day's data. Thus, in the event of a tsunami, it is only necessary for the local weather operator to wait a week, exchange the tiny bubble capsule for a fresh one, and mail the complete digitized memory to Scripps for playback and analysis. For backup, the entire system at Wake is installed in duplicate, except for the copper tube, to which both transducers are connected in parallel.

As presently configured, the system will resolve signals within the pass band to an accuracy of about 2 mm, with an upper magnitude limit of about 2m, set by transducer range. Both variables are adjustable if experience dictates otherwise. The electronics were designed and constructed by Mr. J. McNeil, Delco Electronics, Santa Barbara, who designed previous different types of installations at Wake during the 1970's. Mr. McNeil also participated in the present installation.

Storm Surges--Meteorological Ocean Tides, written by T. S. Murty, published by Canadian Bulletin of Fisheries and Aquatic Sciences, Government of Canada, Ottawa, Canada, K1A 0S9, in 1984: ISBN 0-660-11663-4: 897 pages, price of $41.95 outside Canada.

This lengthy tome presents the detailed history of the study of storm surges, both from the meteorological side and from the oceanographic. Much emphasis is given in the first half of the book to the historical evolution of the analytical and numerical methods for modeling the phenomenon and associated phenomena such as tides and wind waves. The second half of the book is entirely devoted to case histories of meteorological problems and storm surges.

There are only seven chapters. Chapter one is motivational in character, convincing the reader that storm surges have killed enough people and damaged enough property to justify studying them. The weather systems of the globe are described, primarily for North America. The author reviews the evolution of the formulation of the storm surge equations and the corresponding two-dimensional numerical methods. Nonlinear advective terms are included, as are moving boundaries, nested grids, multiple grids, transformed grids, and stretched coordinates. The coverage is limited to vertically integrated models.

Chapter three extends the modeling to two-and-a-half-dimensional models--the 2-D plus a local one-dimensional Ekman model to estimate the vertical distribution of the components of horizontal velocity. This improves the effect of the bottom stress. Three-dimensional finite-difference models with and without stratification are discussed. Splicing of models, for example, a two-dimensional for a bay and a one-dimensional for an estuary discharging into that bay, are described. Finite difference approaches using irregular-grid techniques are discussed; the chapter concludes with some coverage of finite-element methods.

The author looks "under the rug" in chapter four and sweeps over those methods which were not covered in the previous two chapters; many of these methods tend to be of little more than historical interest since the advent of the ubiquitous digital computer. Specifically, the techniques mentioned are analytical, empirical, graphical, statistical, analog (electrical), laboratory and hydraulic experiments, and a bastard combination of hydraulic and numerical modelling that the author terms "hybrid" modeling, to the consternation of any readers versed in electronics.

The emphasis shifts to observations early in chapter five, which covers a pot pourri of hydrodynamic problems. These are so diverse as to justify listing--edge waves, tides, interactions between storm surge and tides, interaction between storm surge and wind waves, and the effect on storm surges of ice or stratification.

In chapter six, the cursory introduction to meteorology given in the first chapter is extensively extended. Extensive examples and collections of statistical information are presented in order to acquaint the reader with the tropical storms and hurricanes which form the main sources for significant storm surges. Various methods of predicting the paths of the storms are described, including the method of images as applied by Choudhury to the Bay of Bengal, modeled as two boundaries almost perpendicular. From the resulting three images, and using two observations to find an initial velocity, the predicted and observed paths differ by less than 20%. The estimation of the forecasting input terms from satellite data is briefly mentioned. Since the book is published in Canada, no reader will be surprised to find that the coverage of storm effects in Canada, and especially the Great Lakes, is very extensive and intensive. However, other notorious places such as the North Sea and Lake Okeechobee, are covered.

Storm surges proper are described as selected case studies in chapter seven. Canada is covered, of course--from east to west. Since much data is presented graphically, for the ease of assimilation by the reader, beware of the inter-relationships between figures. For example, Fig. 7.16 is the reference map for the data given in Fig. 7.20, but that fact is not mentioned in the figure title of Fig. 7.20. Map scales and orientation vectors would have helped many of those figures lacking them. And the pancaking of Figs. 7.17-7.18 does not really add to the ability to do eyeball correlations, relative to the confusion over the titles. Where is the reference map giving the locations for all the interesting data presented in Fig. 7.23? Ah, yes, way back to 7.16.

In this chapter we learn why the author resides on the west coast of Canada: disastrous storm surges do not occur there! After Canada comes the rest of the world: again scales and north arrows would help. Some attempt at mitigation become evident in this chapter, for example, the zoning of the coast of India based on statistical processing of historical data. Finer zonation occurs for the Great Rann of Kutch.

Almost fifty pages of references, not all of which are cited in the text, concludes the book. A subject index would certainly be a boon, but the author begs off with the claim that the table of contents is sufficient. That is hardly true for a voluminous text which covers a huge number of geographical locations at varied places in the book.

This book is one of a new genre. Whereas texts have historically tended to be functional, viz., thermodynamics, seismology, etc., there is a trend towards problem-based books, as in this one. Such coverage is especially valuable to someone just beginning research in that problem area. And such texts synthesize that mass of reprints which the scientist engaged in the field for a long time will have normally have accumulated.

Just to make the foregoing laudatory remarks believable, it seems necessary to include some critical comments. First, a matter of organization. The book would appeal (and be read) by a far wider audience if the very extensive case history material of the second half had been placed first. And, indeed, one likes to think that it was real-world situations which motivated the theoreticians and programmers. But this is, of course, a matter of style.

Computers are a blessing, as evidenced by much of the first portion of the subject book, but perhaps they are also a bane. Or is the typesetting not yet computerized? By this I mean the enormous three-year time gap between the latest references and the appearance of the book--which just happens to be a time of very significant progress on some of the most important topics covered by the book. As examples, scaling, and transforming computational grids as well as formulating the boundary conditions for computer modeling. These seem to be a symptom of the mechanics of production, not any collapse of interest by the author. We do sincerely hope that appropriate improvements will assure that future publications will be up-to-date.

With this book, T. S. Murty has added another fine, useful book to his previous one on tsunamis. The vogue today, at least, in science fiction, seems to be trilogies. We can but hope that the author will choose to undertake the monumental task of completing a trilogy. Maybe there will be prizes for trilogies in science as there are for trilogies in science fiction.

Reviewed by William Mansfield Adams, Sr.

APPLICATION FOR MEMBERSHIP

THE TSUNAMI SOCIETY
P.O. Box 8523
Honolulu, Hawaii 96815, USA

I desire admission into the Tsunami Society as: (Check appropriate box.)

☐ Student ☐ Member ☐ Institutional Member

Name _____ Signature _____

Address _____ Phone No. _____

_____

Zip Code _____ Country _____

Employed by _____

Address _____

Title of your position _____

FEE: Student $5.00 Member $25.00 Institution $100.00

Fee includes a subscription to the society journal: SCIENCE OF TSUNAMI HAZARDS.

Send dues for one year with application. Membership shall date from 1 January of the year in which the applicant joins. Membership of an applicant applying on or after October 1 will begin with 1 January of the succeeding calendar year and his first dues payment will be applied to that year.